*Bulletin of the New Zealand Society for Earthquake Engineering, Vol. 56, No. 3, September 2023*

# SIMPLIFIED SEISMIC LOSS ASSESSMENT USING LIMIT STATE LOSS-INTENSITY MODELS

**Amirhossein Orumiyehei[1] and Timothy J. Sullivan[2]**

(Submitted *November 2021*; Reviewed *April 2022*; Accepted *April 2023*)

**ABSTRACT**

In an effort to provide practicing engineers with simple means of limiting earthquake-induced losses to buildings, this paper extends a simplified damage-state loss vs. intensity approach for estimation of expected annual losses in two ways. Firstly, modifications to allow consideration of a threshold replacement limit state are provided. Secondly, an equation for simplified loss assessment of buildings characterised with a three-damage state loss-intensity model is presented. Furthermore, recommendations are provided for the simplified models associated parameters' values. The proposed approach is trialled for three New Zealand code compliant eccentrically braced frame buildings, and the results compared against those obtained through the PEER framework. It is found that the expected annual loss can be predicted to within 10% of the values obtained via rigorous approaches and opportunities for further research are discussed.

https://doi.org/10.5459/bnzsee.1579

## INTRODUCTION

In New Zealand, efforts are on-going to develop low-damage design guidance that can limit the likely earthquake-induced losses that a building will experience during its lifetime [1,2]. One might convincingly argue that from a life-safety perspective, the performance of buildings in the 2010-2011 Canterbury earthquakes was acceptable [3]. However, the widespread damage and disruption, prolonged in part due to the insurance process and in part due to a drawn out aftershock sequence, would suggest that the engineering community should do more to limit the damage to our buildings and infrastructure [4,5]. Similar observations were made following the 1994 Northridge earthquake in the United States, as well as other recent New Zealand earthquakes in the Wellington and Kaikōura regions, in which relatively few people lost their lives during these events and yet the financial impacts of the earthquake were extensive. In the U.S., the 1994 Northridge earthquake prompted changes in seismic design thinking; first with a SEAOC Vision 2000 document [6] that looked to tailor the likelihood of meeting different limit states with a client's needs and expectations, and later with the development of a performance-based earthquake engineering (PBEE) framework (Porter and Beck 2004) by the Pacific Earthquake Engineering Research Center (PEER), which has developed to FEMA-P58-1 [7] to permit quantification of performance measures such as direct economic losses (e.g. structural damage) and indirect economic losses (e.g. downtime) using probabilistic methods. It is perceived that in New Zealand a more simplified and practice-oriented means of limiting direct losses (i.e. those linked to post-earthquake repair works) would be desirable, and this is the focus of this paper.

The PEER PBEE framework permits rigorous loss assessment of a building and can be realized via the four-stage process described in Figure 1. The four-stages are: (1) hazard analysis to identify the rate of different levels of ground shaking intensity being exceeded at a site, (2) structural analysis to estimate the likely response of the building for a given level of ground shaking intensity, quantified in terms of engineering demand parameters (EDP) such as peak floor acceleration (PFA) or peak inter-storey drift ratio (PIDR), (3) damage analysis to identify the likely damage to the various components in the building for a certain value of EDP, (4) loss analysis from which the repair costs (or other consequences relevant for decision making such as injuries or downtime) are quantified considering the expected damage states for the various components in the building. By integrating the results of these four analysis phases over a relevant range of ground shaking intensity levels, one can identify loss measures for the building such as the expected annual monetary loss (EAL). Full details of the framework are described in FEMA-P58-1 [7].

The PEER PBEE framework described above would clearly represent a significant departure from current structural engineering practice in New Zealand and also overseas. The task of running structural analyses for different intensity levels would not be a significant challenge but analysis stages 3 and 4 will be unfamiliar to most practitioners and execution of probabilistic seismic hazard analysis (likely required for stage 1) is uncommon except for large projects or buildings of high importance such as hospitals. In light of the demanding nature of the PEER PBEE process, a number of proposals have been made to offer simplified alternatives and a selection of these will be reviewed in Section 2. Furthermore, modifications and extensions to the simplified limit state loss-intensity model [8] are then proposed in Section 3. The simplified approach to assess the likelihood of limit state exceedance is outlined in Section 4. The approach adopted to estimate the modified and newly developed simplified loss models' parameters is outlined in Section 5. The accuracy of the simplified loss assessment approach is gauged in Section 6 through its application to a series of case-study buildings and comparison with loss-assessment results obtained from conventional rigorous loss-assessments.

## OVERVIEW OF DIFFERENT SIMPLIFIED METHODS

### Methods That Simplify Structural Analysis Phase

The approach described by FEMA-P58-1 [7] advocates the use of non-linear dynamic analyses as a general approach in the structural analysis phase. However, there are several practical challenges to this, such as (i) the resources and computational

[1] *Corresponding Author, PhD, University of Canterbury, Christchurch, amirhossein.orumiyeh@gmail.com*
[2] *Professor, University of Canterbury, Christchurch, timothy.sullivan@canterbury.ac.nz (Member)*

effort required to run a large number of structural analyses in engineering practice and (ii) the complexity regarding selecting ground motion records which are compatible with the site's seismic hazard.

In light of the challenges of using non-linear dynamic analysis approaches, FEMA-P58-1 [7] does also permit simplified linear structural analyses with correction factors to allow for non-linear response and higher mode effects. Median values of demand obtained from these simplified analyses are paired with empirical values of dispersion to provide the demand values distributions required for analysis stages 3 and 4 of the framework (see Figure 1). Fajfar and Dolšek [10] propose that pushover analysis be used to obtain estimates of the median values of engineering demand parameters (EDP) at a certain level of intensity (IM), which could also be used with empirical values of dispersion to simulate the uncertainty in the IM-EDP relationship. A similar proposal is made by Sullivan et al., [11] who propose use of a displacement-based assessment procedure as a simplified nonlinear static analysis approach. Hwang and Lignos [12] also advocate the use of simplified analyses, considering wavelets in instrumented buildings, to estimate storey-based EDP values for rapid earthquake induced loss assessment of steel buildings at a city-scale. Recently, Orumiyehei and Sullivan (a) [13] have proposed a simplified intensity-EDP relationship that estimates the intensity required to exceed a given limit state for single degree of freedom systems as well as multi-storey reinforced-concrete wall buildings [14].

A number of researchers have aimed to provide information to quantify the dispersion in demand parameters for different structural systems [10,15,16]. In addition, efforts are on-going to quantify the dispersion caused by modelling uncertainty [17-21]. On the other hand, Fox and Sullivan [22] explain why empirical values of demand dispersion may often be inaccurate and propose an alternative means of quantifying this using conditional spectra [23]. However, this approach relies on the use of conditional spectra which may become common in the future but are not currently widely available.

**Methods That Simplify Damage and Loss Analysis Phases**

In the rigorous PEER PBEE approach, the quantities and characteristics of damageable components in a building are required together with relevant component fragility functions in order to identify the likely damage expected for a given value of storey drift or floor acceleration (or other relevant EDP). This process is not only quite time-consuming but may also be problematic for design as it presumes that an engineer will have such data available when typically a detailed inventory of damageable components will only become available at or after construction of the building. Furthermore, once the damage state is established for a component, a repair cost (or loss) function is required to identify the consequences of damage. Sourcing relevant fragility and loss functions may be challenging and intricate for practicing engineers.

A number of proposals have been made to simplify these damage and loss analysis phases. For example, [24] proposed the use of EDP to decision variable (EDP-DV) functions such as those shown in Figure 2 (from [25]). These functions can be formed by combining information on component fragility with information on loss, considering all possible damages, so that the PEER PBEE analysis phases 3 and 4 (Figure 1) can essentially be condensed into a single analysis phase. Furthermore, by grouping components according to non-structural drift-sensitive, non-structural acceleration sensitive and structural (drift sensitive) components considering typical building characteristics, engineers avoid the need for a detailed inventory of damageable components. A key aspect of the EDP-DV functions developed by [24] was that efforts were made to account for component interaction, both when estimating damage and likely repair methods. Figure 2 shows that the EDP-DV functions provide a reasonably simple means of quantifying the expected repair costs for a given storey (expressed in terms of the value of the storey) as a function of either drift or floor acceleration.

More recently, Dhakal and Saha [26] have proposed a similar approach for use within a loss optimisation seismic design process. Figure 3 illustrates what they refer to as generic normalized floor level loss functions, providing similar information to that provided by Ramirez and Miranda [24] but indicating also uncertainty in the loss values. It should also be noted that the process used to arrive at these floor level loss functions is different to that followed by Ramirez and Miranda [24] and for more details, readers should refer to [26] and [27]. Furthermore, Shahnazaryan et al. [28] have also proposed an algorithm based on which a software has been provided to estimate the storey-loss functions for a specific building. O'Reilly and Calvi [29] have developed an approach to quantify the non-structural components' risk and consequently, classifies these elements in different structural systems. The availability of such tools with the capability of adaptations to different standards can make the simplified loss assessment procedure and the subsequent informed decision-making process easier.

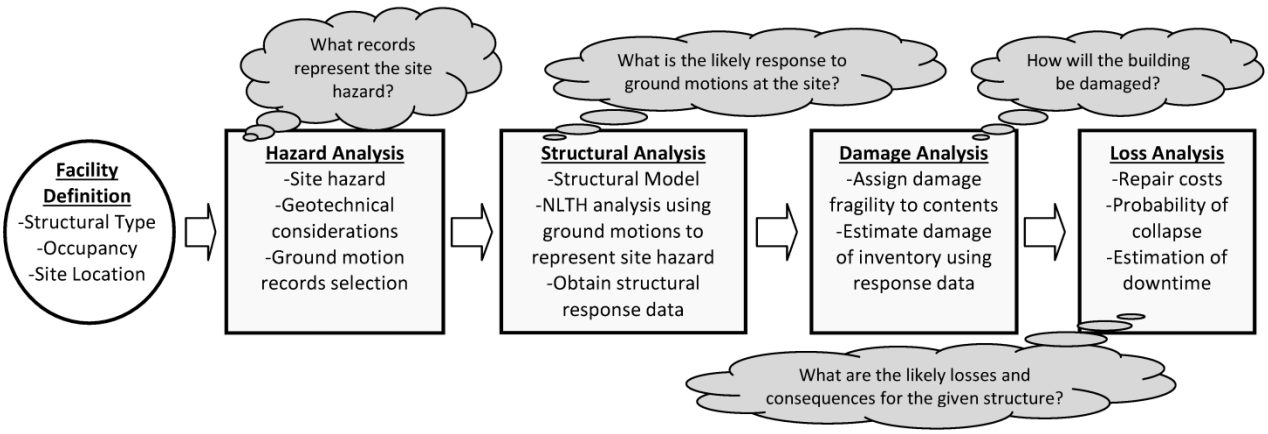


***Figure 1: Overview of the four stages of the PEER PBEE framework (from [9]).***

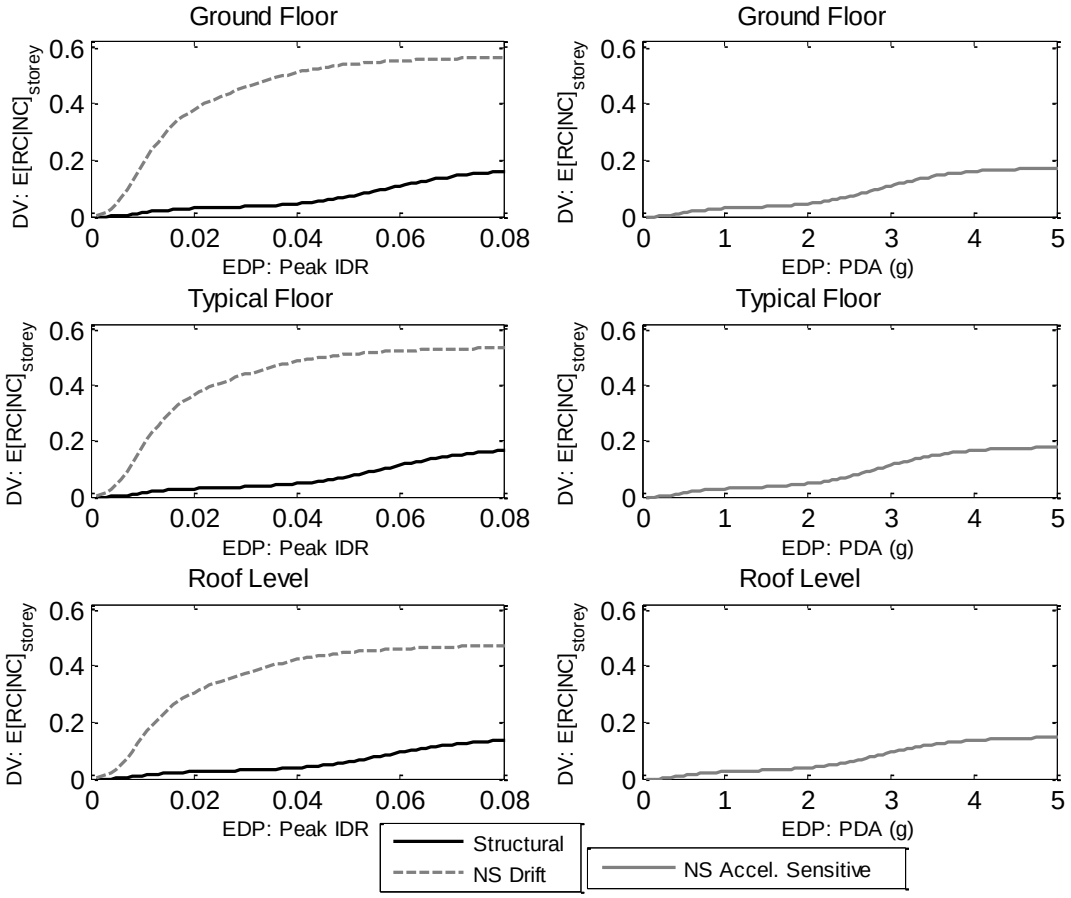


***Figure 2: EDP-DV relationships (after Ramirez and Miranda [24]) between interstorey drift ratio (IDR) and expected repair cost (RC) (left) and peak floor acceleration (PFA) and repair cost (right), conditioned on no-collapse E[RC\|NC], for a four-storey reinforced concrete space frame (from Welch et al.. [25]).***

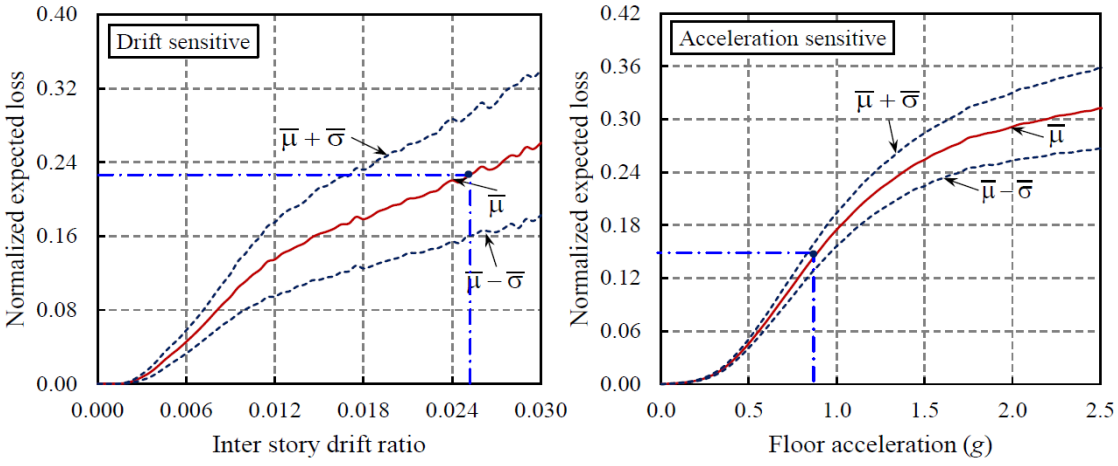


***Figure 3: Generic normalized floor level loss functions (from Dhakal and Saha [26]).***

**Limit State Loss Approaches**

Seismic design has traditionally been undertaken with reference to different limit states. However, there are a range of different limit states defined in the literature and national standards. In New Zealand, reference is made to a serviceability limit sate (SLS) and an ultimate limit state (ULS) for typical buildings [30]. However, a serviceability limit state (SLS), damage control limit state (DCLS), and collapse avoidance limit state (CALS) are considered for bridges [31]. In Italy, the following four limit states are considered: (i) operational limit state, (ii) damage limitation limit state, (iii) life-safety limit state, and (iv) collapse prevention limit state. In a code for displacement-based design, Sullivan et al. [32] instead refer to three limit states: (i) No-damage, (ii) Repairable damage (in which a certain amount of repairable damage is acceptable but cost should be significantly less than replacing building) and (iii) No-collapse.

Whilst there are clearly some differences in opinion about the definition of limit states, they are inherently linked to physical damage states similar to those identified in analysis phase 3 of the PEER PBEE approach (refer Figure 1). Furthermore, the intensity that causes a certain limit state to develop is likely to

be an intensity level of relevance to the loss assessment process. Given that practitioners will also be familiar with assessing a structure to specific limit states, [33] proposed that the PEER PBEE procedure could be simplified by evaluating the losses and likely return period of four limit states [34], as illustrated on the right side of Figure 4 (adapted from Welch et al. [33]). Furthermore, Welch et al. [33] propose that displacement-based assessment could be used to assess the likelihood of these four different limit states considering the uncertainty in demand and capacity, and that the EDP-DV functions of Ramirez and Miranda [24] could be used to quantify the losses at the different limit states. Note that Welch et al. [33] adopt a set of EDPs and employ EDP-DV functions (presented in Figure 2) to compute the expected annual loss.

By making the simplifications described above, Welch et al. [33] defined the mean annual frequency (i.e. inverse of return period) of four different loss levels and then through integration (taking the area under the curve in Figure 4) the expected annual loss could be estimated. The left side of Figure 4 shows the equivalent process followed in the PEER PBEE procedure [7]. Multiple assessments are required over a range of intensity levels and the expectation is that a sufficiently wide range of intensity levels is considered in order to properly assess the expected annual loss. Comparing the left and right sides of Figure 4, it can be seen that focusing on limit states reduces the amount of analysis work to compute the expected annual monetary loss.

Simplified limit state loss approaches appear to have gained popularity in Italy. The Italian Ministry of Infrastructure and Transport recently passed legislation (Ministerial Decrees 58 and 65, MIT (2017, 2017a)) that foresees seismic performance classification via loss assessment. Attachment A of the decree prompts the use of a limit state approach similar to that shown on the right side of Figure 4, together with values of loss (expressed as a fraction of the building replacement cost) that are tabulated for different limit states. By offering a simplified methodology, the Italian industry now permits simplified loss assessment for seismic performance classification of buildings throughout Italy. Furthermore, the Italian government has sought persuasive policies to facilitate residential building retrofit. These policies include “Sismabonus”, which provides a tax deduction of up to 96 thousand Euros (proportional to the seismic class grade) in 5 years [35]. While the approach of Welch et al. [33] does reduce the amount of work required to assess losses as compared to the PEER PBEE approach, Sullivan [8] proposed an even simpler method that reduces the problem down to assessment of two limit states: (i) a zero-loss limit state and (ii) a replacement limit state. This simplifies the loss assessment greatly because an inventory of damageable components, fragility functions and loss functions are no longer required, given that the loss at the zero-loss limit state is zero (as the name suggests) and the loss at the replacement limit state corresponds to the replacement value of the building. Furthermore, by making assumptions that losses vary linearly with intensity between the zero-loss and replacement limit states and that the seismic hazard curve can be approximated with a power law at intensity levels close to the limit states, the expected annual loss (EAL) can be computed from a single equation, as shown in Equation 1 (adapted and rearranged from Sullivan [8].

$$EAL = \frac{\left(\frac{1}{T_{R,0}} - \frac{IM_{rep}}{IM_0} * \frac{1}{T_{R,rep}}\right)}{\left(\frac{IM_{rep}}{IM_0} - 1\right)\left(1 - \frac{\ln\left(\frac{IM_{rep}}{IM_0}\right)}{\ln\left(\frac{T_{R,rep}}{T_{R,0}}\right)}\right)} - \frac{\left(\frac{1}{T_{R,0}} - \frac{1}{T_{R,rep}}\right)}{\left(\frac{IM_{rep}}{IM_0} - 1\right)} + \frac{1}{T_{R,rep}} \quad (1)$$

where, $IM_0$ and $IM_{rep}$ are median intensity levels of ground motion assessed to cause first exceedance of the zero-loss and replacement limit states, respectively, and $T_{R,0}$ and $T_{R,rep}$ are the corresponding return periods of these intensity levels.

The EAL computed from Equation 1 has units of loss expressed as a fraction of the building replacement cost. Cardone et al. [36] also proposed a refinement of the above approach that does away with the need for assessment of the replacement limit state but does require information on the rate at which losses vary with intensity. For that purpose, it was assumed that the minor damages might be reflected by introducing $q$ as the parameter that could be considered equivalent to the excess in an insurance company policy. Furthermore, allowance for a loss “threshold” ($Th$) was set forth, recognising that building owners will often choose to replace their buildings even though the cost of repair would be less than replacement [37,38]. In order to account for these thresholds, the slope ($m$) of the limit state loss-intensity relationship was modified as illustrated in Figure 5. Cardone et al. [36] recognised that the threshold value increases the slope but does not cause a step change in the loss-intensity curve because, for a given seismic intensity, a number of earthquakes at that intensity level may prompt replacement but a number may not and thus the impact of a threshold on the curve is gradual. Regression analysis was employed to estimate the loss-intensity curve’s slope using the results of loss analyses from PACT [39] for 4-, 6-, and 8-storey reinforced concrete frame case study buildings typical of Italian construction.

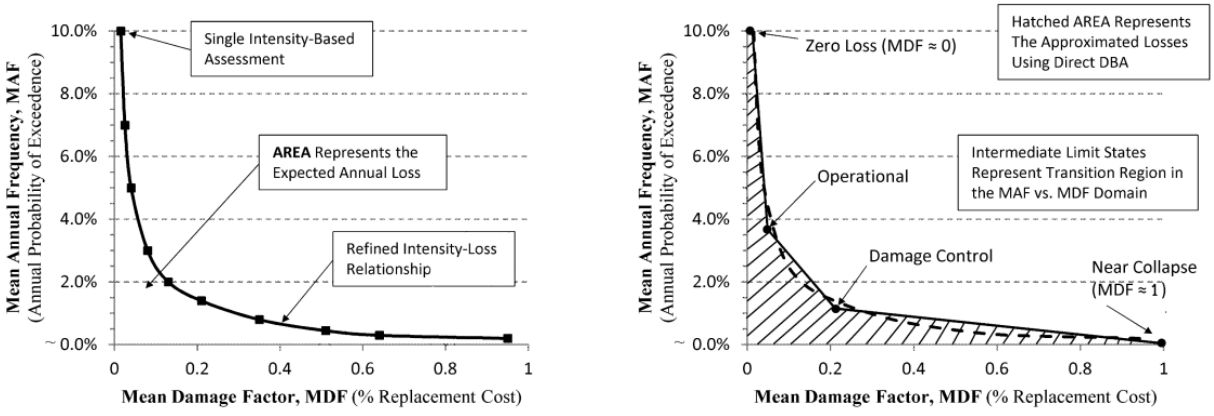


***Figure 4: Comparison of expected annual loss calculation using the PEER PBEE methodology (left) and simplified four limit state approach (right) (from Welch et al. [33]).***

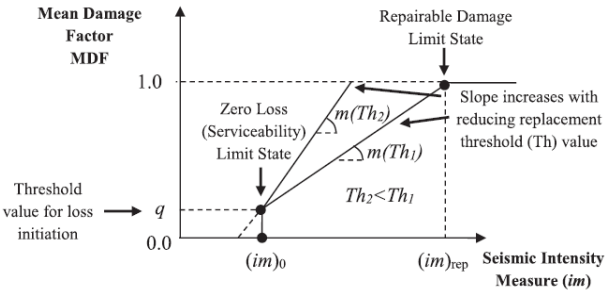


***Figure 5: Development of limit state loss-intensity accounting for loss thresholds [36].***

With increasing awareness of the relevance of expected annual loss (EAL) in assessment, O'Reilly and Calvi [40] have proposed a simplified procedure to specify the required strength and stiffness that limits the acceleration and deformation induced losses. Shahnazaryan and O'Reilly [41] also propose an integrated performance-based seismic design (IPBSD) process using the mean annual frequency of collapse (MAFC) and expected annual loss (EAL) as alternatives for strength and drift requirements checked in current seismic design standards.

Reviewing recent developments, it is noted that while the approach of Cardone et al. [36] to use the slope does simplify the assessment, it also relies on knowledge of the slope factor and has difficulty adapting to cases where building characteristics or design criteria will have altered the vulnerability of the building for different limit states. On the other hand, the approach of Shahnazaryan et al. [28] appears to rely on computer coding that they have made available on-line. Whilst this type of approach promises accuracy, it is considered that further development of simplified limit-state loss methods will help practitioners to either permit the relative performance of different building solutions to be made or help identify limit state design intensity levels that can be adopted to effectively limit losses. As such, in the following section, the limit-state loss assessment approach of Sullivan (2016) is developed to incorporate and improve the bi-linear loss model, which is called a two-damage state, and a three-damage state loss-intensity model are to permit more accurate practice-oriented loss assessment.

## IMPROVING THE SIMPLIFIED LIMIT STATE-LOSS ASSESSMENT APPROACH

To compute the expected annual loss according to Equation (1), one must first identify the engineering demand parameters (EDPs) that correspond to the onset of the two limit states. Secondly, the challenge is then to identify the intensity and return period of ground shaking that would cause these values of EDP to be reached, and thirdly, to quantify the uncertainties associated with the estimation of the assessed limit state intensities. Ideally, codes would define criteria such that the limit states used in design correspond to the initiation of the different limit-state loss levels defined earlier. In reality, however, it is recognized that our understanding of the drift and acceleration that triggers different loss levels is still developing. For the zero-loss (ZL) limit state, one might consider the median drift (or acceleration) capacity of the most vulnerable element in the building. This is likely to be a non-structural element, such as plasterboard partition walls [42]. For the replacement limit state, more research is required to quickly estimate an EDP that corresponds to the point at which the cost to repair the building is the same as the cost of replacement. One could tentatively adopt ultimate limit state drift limits, as proposed by Sullivan [8] and mentioned in ASCE-41 [43], but owing to differences between building typologies, there is likely to be considerable uncertainty introduced via this approach. A more accurate means of identifying the engineering demand parameters expected to trigger the zero loss and replacement limit states could be to utilize floor-loss functions, such as those proposed by Ramirez and Miranda [24] and Dhakal and Saha [26], illustrated earlier in Figure 2 and Figure 3, respectively.

To allow for a threshold level of damage to be considered when assessing the replacement limit state, the intensity, $IM_{thr}$, that would push the building damage to the threshold point could also be found using floor-loss functions, with the mean loss beyond this intensity level then taken equal to 1.0 (i.e. replacement), as shown in Figure 6. It was noted earlier (as pointed out by Cardone et al. [36]) that actual intensity versus loss will tend to show a gradual increase in loss owing to the variability in damage expected in a building subject to different earthquakes of the same intensity. However, this variability, which is not reflected in Figure 6, will be accounted for approximately when probabilistically dealing with uncertainties, as described later in the paper.

Recognising the current uncertainty that exists in the relationship between design limit states and loss levels, Figure 6 refers to the median loss functions as damage state loss-intensity relationships. For the two-damage state loss model shown in Figure 6(a), a closed-form solution for the EAL that utilizes a zero-loss and a replacement threshold limit state can be obtained using a similar approach to that of Sullivan [8] (as demonstrated in Appendix A) which leads to Equation (2):

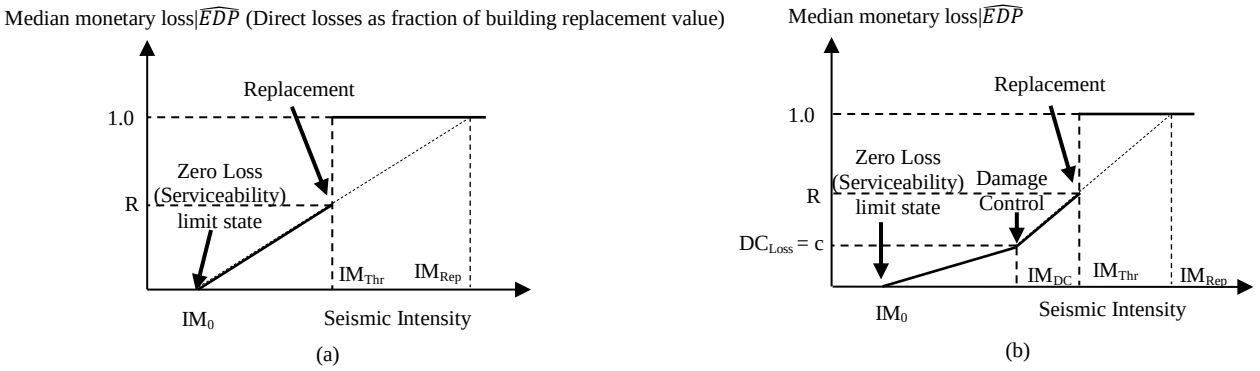


***Figure 6: Idealised (a) two-damage state and (b) three-damage state loss-intensity (median repair cost) curves incorporating a threshold replacement limit state (before accounting for the uncertainties in demands).***

$$EAL = R\frac{\left(\frac{1}{T_{R,0}} - \frac{IM_{Thr}}{IM_0}\frac{1}{T_{R,Thr}}\right)}{\left(\frac{IM_{Thr}}{IM_0} - 1\right)\left(1 - \frac{\ln\left(\frac{IM_{Thr}}{IM_0}\right)}{\ln\left(\frac{T_{R,Thr}}{T_{R,0}}\right)}\right)} - R\frac{\left(\frac{1}{T_{R,0}} - \frac{1}{T_{R,Thr}}\right)}{\left(\frac{IM_{Thr}}{IM_0} - 1\right)} + \frac{1}{T_{R,Thr}} \quad (2)$$

where, $IM_0$ and $T_{R,0}$ are, respectively, the ground motion's intensity and limit state exceedance's return period associated with the zero loss limit state; $IM_{Thr}$ and $T_{R,Thr}$ are the ground motion's intensity and replacement threshold limit state exceedance return period (the return period is achieved by taking the inverse of the annual rate obtained from Equation 5), respectively; $R$ is the loss ratio for the replacement threshold limit state (the approach of Sullivan [8] implicitly assumed that R = 1).

In the loss assessment process, the impact of loss at high frequency events is not only significant, but in some cases may dominate the expected annual loss calculation [44]. Furthermore, the loss-intensity curve's gradient may vary naturally as a function of the quantity of different components, damage states, and corresponding repair costs (losses). In such cases, the loss-intensity curve could be better modelled by applying a three-damage state-loss curve, illustrated in the right side of Figure 6. Furthermore, the structural design team may decide to consider a so called damage control limit state (a limit state that first appears to have been introduced by Priestley et al. 2007) to limit the likelihood of significant interruption in building functionality. By introducing a new design limit state, such as the damage-control limit state (DCLS), that aims to ensure that repair costs (losses) are limited for a certain return period of shaking, the loss-intensity curve could be expected to change into a three-damage state loss model, shown on the right side of Figure 6. To account for this, Equation (3) is formulated for simplified loss assessment using a three-damage state loss function in which the designer's chosen loss ratio ($c$) associated with an intermediate limit state (e.g. damage control) is introduced as illustrated in Equation (3) and the right side of Figure 6. Note that even though Figure 6 indicates that the slope of the loss-intensity curve increases after the DCLS intensity, this is just indicative and the slopes before and after DCLS could be affected by the structural and non-structural systems present, as well as the design approach adopted for the building.

$$EAL = c\frac{\left(\frac{1}{T_{R,0}} - \frac{IM_{DC}}{IM_0}\frac{1}{T_{R,DC}}\right)}{\left(\frac{IM_{DC}}{IM_0} - 1\right)\left(1 - \frac{\ln\left(\frac{IM_{DC}}{IM_0}\right)}{\ln\left(\frac{T_{R,DC}}{T_{R,0}}\right)}\right)} - c\frac{\left(\frac{1}{T_{R,0}} - \frac{1}{T_{R,DC}}\right)}{\left(\frac{IM_{DC}}{IM_0} - 1\right)} + (R-c)\frac{\left(\frac{1}{T_{R,DC}} - \frac{IM_{Thr}}{IM_{DC}}\frac{1}{T_{R,Thr}}\right)}{\left(\frac{IM_{Thr}}{IM_{DC}} - 1\right)\left(1 - \frac{\ln\left(\frac{IM_{Thr}}{IM_{DC}}\right)}{\ln\left(\frac{T_{R,Thr}}{T_{R,DC}}\right)}\right)} - \left(\frac{R-c}{\frac{IM_{Thr}}{IM_{DC}} - 1} - c\right)\left(\frac{1}{T_{R,DC}} - \frac{1}{T_{R,Thr}}\right) + \frac{1}{T_{R,Thr}} \quad (3)$$

where, $IM_{DC}$ and $T_{R,DC}$ are, respectively, the ground motion intensity and corresponding return period (reverse of annual rate achieved from Equation 5) that trigger the damage control limit state, and $c$ is the associated loss ratio (shown as Damage Control Loss in Figure 6 (b)); the other parameters have been defined previously.

The newly derived Equations (2) and (3) are considered to represent a valuable contribution to the state of the art, enhancing the accuracy of limit-state loss assessment. Note that the proposed solutions rely on an assessment of the intensity, and associated annual probability of exceedance, at which key limit states are likely to be reached; this implies that either two or three limit states need to be assessed, depending on whether one is applying the two- or three-damage state loss-intensity models. Recommendations for defining the loss ratio at each limit state are provided in Section 6.4.1. One aspect that has not been mentioned to this point is the treatment of uncertainties in the simplified assessment process, discussed next.

## QUANTIFICATION OF THE LIKELIHOOD OF LIMIT STATE EXCEEDANCE

From Equations (2) and (3) it can be seen that the EAL is a function of the annual frequency of exceedance of different limit states. According to the SAC-FEMA approach [45] and the formulation proposed by Vamvatsikos [46], the annual frequency of exceeding a specific limit state can be estimated using the hazard value ($\mathrm{H}(S_a)$) computed in Equation (4), that indicates the rate of exceeding an intensity measure ($S_{a,c}$) that pushes the building beyond the limit state capacity. Vamvatsikos [46] put forward an approach that applies a second order fit of the hazard in log space (illustrated in Equation (4)) to enhance the estimation of the annual frequency of exceeding a given limit state, as illustrated in Equation (5).

$$\mathrm{H}(S_a) = k_0 \exp(-k_2 \ln^2(S_a) - k_1 \ln S_a), \quad (4)$$

where, $k_0$, $k_1$, and $k_2$ are the coefficients adapted to estimate the hazard curve as the mean annual frequency ($\mathrm{H}(S_a)$, illustrated in Equation (4)), at which different levels of shaking intensity, $S_a$, are exceeded at a site; the equation for computing the limit state's rate of exceedance proposed by Vamvatsikos (2012) to estimate the annual rate of exceeding a limit state ($\lambda_{LS}$) is given by Equation (5), where the parameter $p$ is defined in Equation (6).

$$\lambda_{LS} = \sqrt{p}\, k_0^{1-p} [\mathrm{H}(S_a)]^p \exp\left[\frac{k_1^2}{4k_2}(1-p)\right] \quad (5)$$

$$p = \frac{1}{1 + 2k_2(\beta_{Tot}^2)}, \quad (6)$$

where, $\beta_{Tot}$ is the total dispersion (measure of uncertainty) that can be computed considering the dispersion in demand, $\beta_D$, and capacity, $\beta_C$, as recommended by Bakalis and Vamvatsikos [47] and illustrated in Equation (7).

$$\beta_{Tot} = \sqrt{\beta_D^2 + \left(\frac{\beta_c}{b}\right)^2} \quad (7)$$

where, $b$ is a coefficient used in the relationship that describes the rate of variation in displacement (ductility) demand as a function of seismic intensity. Traditionally, this value was taken as 1.0, but recently, Orumiyehei and Sullivan [14] proposed new 'b' values as a function of the hysteretic characteristics of buildings, which are provided in Table 1.

*Table 1: Intensity-demand coefficients,* **b***, and associated dispersion,* **β***, for different hysteretic models (from [14]).*

| Period | Bilinear | | Takeda | | Flag (λ = 5.67) | | SINA | |
|---|---|---|---|---|---|---|---|---|
| T(s) | b | β | b | β | b | β | b | β |
| **0.2 ≤ T < 0.6** | 1.28 | 0.12 | 1.57 | 0.24 | 1.86 | 0.34 | 2.50 | 0.42 |
| **0.6 ≤ T≤ 3.5** | 1.12 | 0.10 | 1.26 | 0.12 | 1.49 | 0.12 | 1.38 | 0.17 |

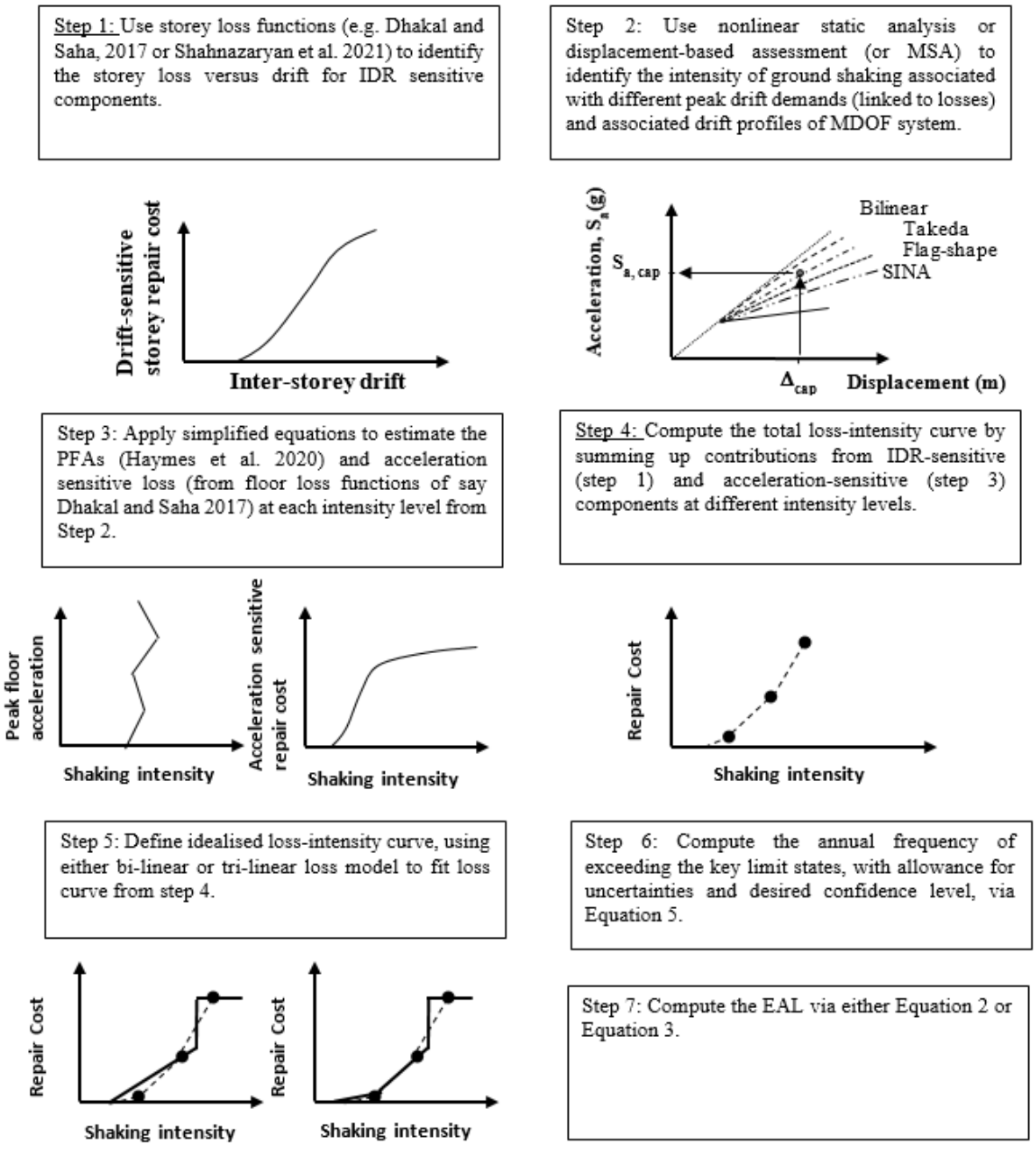


*Figure 7: Overview of simplified loss assessment procedure.*

## IDENTIFYING LIMIT STATES FOR LOSS ASSESSMENT

To identify drift and acceleration limits that can be linked to key loss states the process illustrated in Figure 7 is followed. This is described in the following paragraphs. As is seen later in Section 6, the parameters required to implement the approach may be estimated through either simplified or comprehensive analysis approaches.

To compute the loss and define key limit states, the loss functions presented by Dhakal and Saha [26] (or the approach followed by Shahnazaryan [28]) can be adopted to first quantify the repair cost for each storey as a function of drift, for drift-sensitive elements, as stated in step 1 of Figure 7. To do this,

the engineer could first consider the quantity and fragility of the different structural and non-structural components in the building, but Dhakal and Saha (2017) provide guidance for generic functions that depend on building typology. The intensity at which different levels of loss are reached in the drift-sensitive elements can then be assessed via structural analyses (Step 2 in Figure 7). The non-linear static analysis method of Eurocode 8 (CEN 2004), displacement-based assessment, or other simplified structural analysis methods would normally be recommended for this purpose. For the case study buildings examined in this work, the displacement profile proposed by O'Reilly and Sullivan [48] for eccentrically braced frames was employed to assess drift-sensitive loss at each storey at a given intensity (illustrated in step 2 of Figure 7) using the generic floor loss functions from Dhakal and Saha [26]. Alternatively, the median value of maximum storey drift and acceleration found from simplified or rigorous methods could be applied to building-specific loss functions [24] to build up the intensity-loss curve.

To estimate the losses stemming from damage to acceleration-sensitive components, Step 3 in Figure 7 indicates that the peak floor acceleration demands at different levels of intensity should be estimated. There are a range of methods available for the estimation of peak floor accelerations, including guidelines in FEMA P-58 and other codes. However, as current code methods are known to have limited accuracy [34], alternative methods, such as the approach of Haymes et al. [49] could be used to find the peak floor acceleration (PFA) demands. Whilst a modal response spectrum method for the prediction of peak-floor acceleration (PFA) demands should work well for elastic building response, it is expected to overestimate PFAs when significant inelastic response develops in the structure. As such, future research could investigate the benefits of adopting alternative, emerging methods for estimation of PFA demands.

In this work, the acceleration profile proposed by Haymes et al. [49] was applied to estimate the acceleration-sensitive loss at each storey (as illustrated in step 3 of Figure 7) in which the floor acceleration response spectrum is obtained as:

$$FA_{i,j} = \Gamma_i \phi_{i,j} S_{GA}(T_j, \xi_{str}) \quad (8)$$

where, $FA_{i,j}$ is the floor acceleration spectrum at the j$^{th}$ mode shape coordinate and i$^{th}$ floor; $\Gamma_j$ is the j$^{th}$ mode's participation factor, $\phi_{i,j}$ is the j$^{th}$ mode shape coordinate at the i$^{th}$ storey, $S_{GA}(T_j, \xi_{str})$ is the ground acceleration response spectral ordinate at the period of vibration of j$^{th}$ mode ($T_j$) and the structural damping of $\xi_{str}$ (or alternatively 5%). Note that the $PFA_i$ at the i$^{th}$ storey can be found by square root of sum of squares of $FA_{i,j}$ obtained accounting for different mode contributions (with the first two modes in each direction considered for the case study buildings).

With the PFA at each storey computed for different levels of intensity, then the losses due to damage to acceleration-sensitive components can be found using storey-loss functions, such as those presented by Dhakal and Saha (2017). By summing together the drift-sensitive losses with the acceleration-sensitive losses, then a total loss versus intensity relationship can be established, as per Step 4 in Figure 7. Subsequently, the loss-intensity curve can be inspected to identify the intensities at which key limit states are exceeded.

Depending on the building being assessed, either the two-damage or three-damage state idealized loss-intensity model could be used to fit the total-loss curve, as illustrated in step 5 of Figure 7. Subsequently, the annual frequency of exceedance of the key limit states can be estimated by applying Equation (5) demonstrated in Section 4, as illustrated in step 6 of Figure 7. In Step 7, the information on the key limit states is implemented in Equation (2) or Equation (3) (depending on the choice of the loss model) and the expected annual loss is computed. As part of this, the approach proposed by Vamvatsikos [46] is employed to quantify the likelihood of exceeding the corresponding limit state as illustrated previously in Section 4.

## TESTING THE PERFORMANCE OF THE PROPOSED SIMPLIFIED LOSS ASSESSMENT PROCEDURE THROUGH APPLICATION TO CASE STUDY BUILDINGS

In order to gauge the accuracy of the proposed simplified loss assessment procedure, the rigorous loss assessment process following the PEER framework (i.e. FEMA-P58-1 [7]) is first applied to a series of case study buildings to provide a benchmark for later comparison with loss estimates obtained via the simplified approach.

### Description of Case Study Buildings

Three buildings with steel EBFs; 4-storey and 12-storey buildings located in Wellington, and a 4-storey building located in Christchurch, are designed in accordance with New Zealand standards [30,50,51]; the architectural layouts compatible with office buildings were considered. The layout corresponding to the 4-storey building is composed of five bays in one direction and three bays in the other with 8 m bay lengths (24 m by 40 m). However, the 12-storey building's layout is four and six bays in the two orthogonal directions (32 m by 48 m), as illustrated in Figure 8. The geometrical characteristics of the Christchurch and Wellington 4-storey buildings are identical.

In order to represent the New Zealand design state of practice, design assumptions were made in line with what is understood to be local practice. Furthermore, a finite element model in the structural analysis program SAP (2000) [52] was developed to permit modal response spectrum analyses and calculate demands. The New Zealand standards were used to compute dead, live, wind, and earthquake loads [30,50,53]. Moreover, the earthquake loads were computed employing the modal response spectrum analysis method recommended by the New Zealand standard (NZS 1170.5, 2004) [30] considering a generic site with site soil class C and hazard factor of 0.4 for Wellington, and site soil class D and hazard factor of 0.3 for Christchurch**,** and steel member sizes and connections were defined following the New Zealand steel structure standards [51]. The design ductility factor was taken equal to 3 for all case study buildings, which is considered to be the maximum allowed ductility factor for the structures categorized as limited ductile as per recommendation by NZS 3404:1/2 (2007) [51] for buildings with office functions. The yield strength coefficient was found to be 0.17 and 0.08 for the 4- and 12-storey buildings located in Wellington, and 0.20 for the 4-storey building in Christchurch. Note that the active link lengths were chosen to be small enough to ensure shear behavior governs. Table 2 lists the fundamental periods obtained during the design procedure for each case study building. The design process with more details is provided in Appendix B.

### Structural Modelling for Non-Linear Analyses

To proceed with the structural analysis phase for rigorous loss assessment according to the FEMA P-58 approach, a 2-D model was developed in OpenSEES [54] for each case study building. To account for P-Δ effects, large displacement analysis was run and a gravity column (providing no lateral stiffness to the system) that carries half of the floor weight at each level was included. The gravity column was constrained horizontally to the seismic frame at each level assuming that the floors had sufficient stiffness to act as rigid diaphragms (in-plane) at each level.

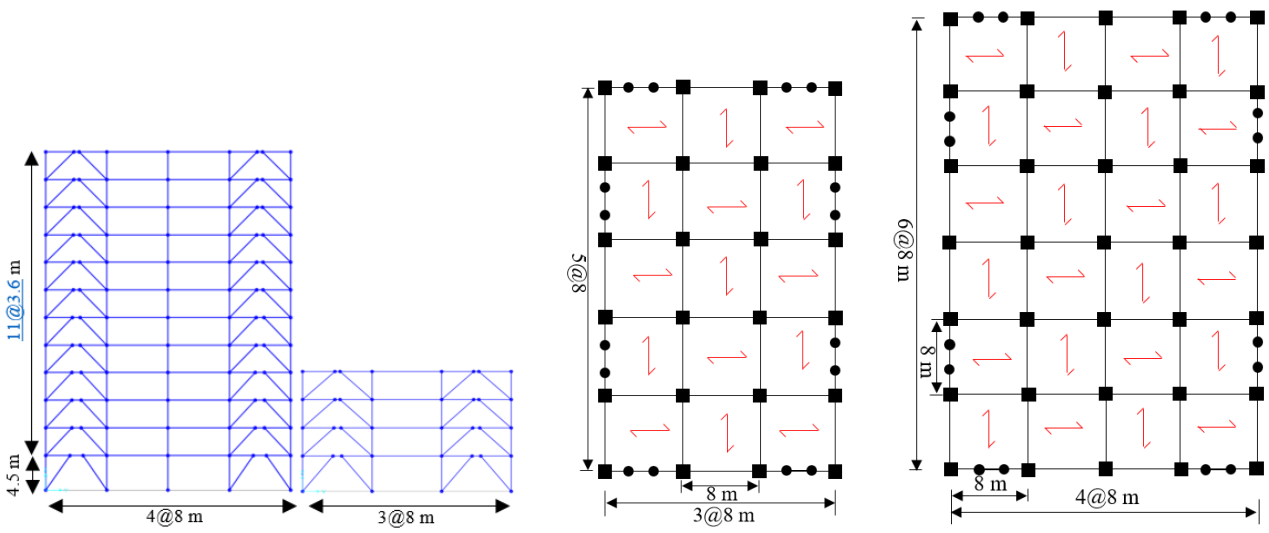


***Figure 8: Presenting (a) elevation of 12-storey (b) elevation of 4-storey (c) plan layout of 4-storey, and (d) plan layout of 12-storey case study buildings.***

***Table 2: Fundamental period of vibration, T(s), for different case study buildings.***

| Structural system | Wellington | | Christchurch |
|---|---|---|---|
| | 4-storey, $T_1$ (s) | 12-storey, $T_1$ (s) | 4-storey, $T_1$ (s) |
| **Eccentric braced frame** | 0.61 | 2.35 | 0.57 |

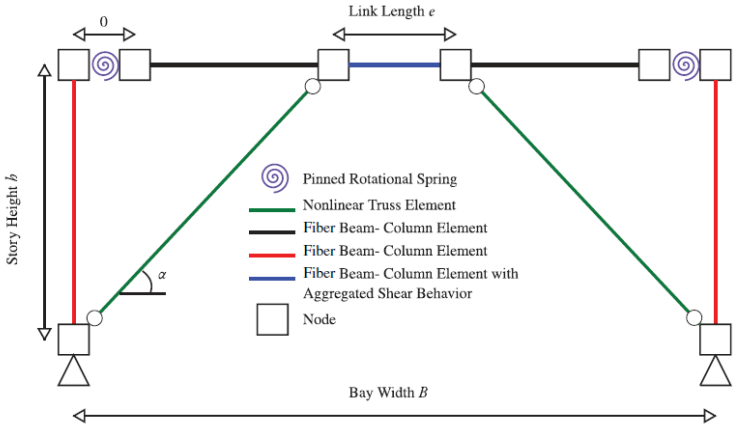


***Figure 9. Eccentric braced frame 2-D model developed in OpenSEES (O'Reilly et al. [48]).***

The Rayleigh damping with tangent stiffness proportional terms was adopted with 5% damping specified on 1st and 2nd modes for both the 4- and 12-storey buildings. This damping model is arguably not the most appropriate and alternative damping models could be more reasonable (see, for example De Francesco and Sullivan [55]). However, the model adopted is not likely to have affected the main conclusions reached in this work related to simplified loss assessment.

The modelling methodology developed by O'Reilly and Sullivan [56] for EBF structures was followed, as illustrated in Figure 9. As such, force-based beam-column elements using fiber sections aggregated with a bilinear shear behavior were adopted. Beam-column connections as well as brace-beam and brace-base connections were assumed pined. These assumptions are in line with prior research efforts [57,58]. Confidence in both the OpenSEES and SAP2000 models was obtained by comparing mode shapes and periods of vibration, which were found to be closely aligned.

To estimate the structural demands, multi stripe analyses (MSA) [59] were conducted. For that purpose, a set of 20 ground motions (with both horizontal components) were used at each of 9 intensity levels (stripes) for time history analysis of the Wellington case study buildings, and 15 intensity levels for the case study building located in Christchurch. The hazard curve for each case is illustrated and compared with NZS 1170.5 associated hazard in Figure 10; the ground motions were

selected by Yeow et al. [60] using the generalized conditional intensity measure approach [61]. Figure 11 (a), (b), and (c) illustrate the acceleration response spectrum corresponding to $T_1$=1.0 s and 2.0 s for ground motions selected at the fourth hazard level in Wellington and also 1.0 s for Christchurch and also compares with the acceleration response spectrum provided by NZS 1170.5. The NZ standard NZS1170.5 (2004) 500 year return period design intensity is also shown and presents similar spectral acceleration intensity except for Christchurch 1.0 s, which is slightly larger than the mean of ground motions' response spectrum, as illustrated in Figure 11.

The maximum inter-storey drift ratio (IDR) and peak floor acceleration (PFA) were recorded for each ground motion at each stripe of intensity. Figure 12 illustrates the maximum IDR and PFA demand profile, and also the corresponding median in addition to 16$^{th}$ and 84$^{th}$ percentile values (median plus/minus one standard deviation), for all three case study buildings responding to ground motions compatible with 500 year return period demands. It is seen that the drift and acceleration demand are larger for the Wellington 4-story case study building than those found for the Christchurch 4-storey building. This is in line with the acceleration intensities found from seismic hazard analysis. Furthermore, the median drift demand obtained for each case study is considereably smaller than 2.5% which is indicated by New Zealand standard (NZS 1170.5) as the ultimate limit state drift limit. This occurs because of various additional provisions in the standard, and in general it was found that the design process achieved the intended response as the drift demand found from analysis.

### Loss Assessment Using PEER Approach

To undertake rigorous loss assessment according to the FEMA-P58-1 [7] procedure (also referred to as the PEER approach), fragility functions for components compatible with New Zealand detailing that are available in the literature were adopted [60]. The fragility functions required for shear links in eccentrically braced frames were taken from the approach of O'Reilly et al. [62] and the consequence functions compatible with New Zealand detailing reported by Sullivan et al. [63]. In the case that appropriate fragility functions could not be found, the fragility and consequence functions recommended by FEMA-P58-1 [7] were applied. A loss threshold of 0.40 for all case study buildings, consistent with the simplified loss assessment approach, was specified when applying the rigorous loss assessment. This value was found as the loss ratio corresponding to 3% drift and the associated peak floor acceleration demands following the approach outlined by Dhakal and Saha [26] considering both drift and acceleration sensitive elements. There is uncertainty as to whether this is a suitable threshold but there is also an expectation that if a building in New Zealand undergoes a peak drift demand of 3%, it is likely to be replaced. Furthermore, according to Elwood et al. [38], a large number of damaged buildings with a required repair cost ratio of less than 0.4 were demolished following the Canterbury earthquakes and thus the number is not considered low. Note that FEMA-P58-1 [7] applies 50% as the replacement threshold but it also states that owners have decided to replace their properties if the corresponding monetary loss exceeded 40% according to the previous studies.

The component inventory used for the case study buildings is composed of three main categories of elements. The first category, called structural elements, refers here to the active shear links for the EBF frames. The second category of elements are nonstructural drift-sensitive components, which includes partitions, cladding, glazing and stairs. The third category of elements here are nonstructural acceleration-sensitive elements and is composed of the suspended and braced ceilings, water pipe system, sprinklers, elevator, and HVAC. Among the drift sensitive components, partitions are the most vulnerable components with the first damage state possessing a median drift capacity of 0.27% (the median minus one standard deviation (IDR=0.17%) is considered equivalent to a zero-loss limit state drift capacity). Furthermore, suspended ceilings with 8 m length are the most fragile acceleration sensitive components with median peak-floor acceleration capacity of 0.46 g.

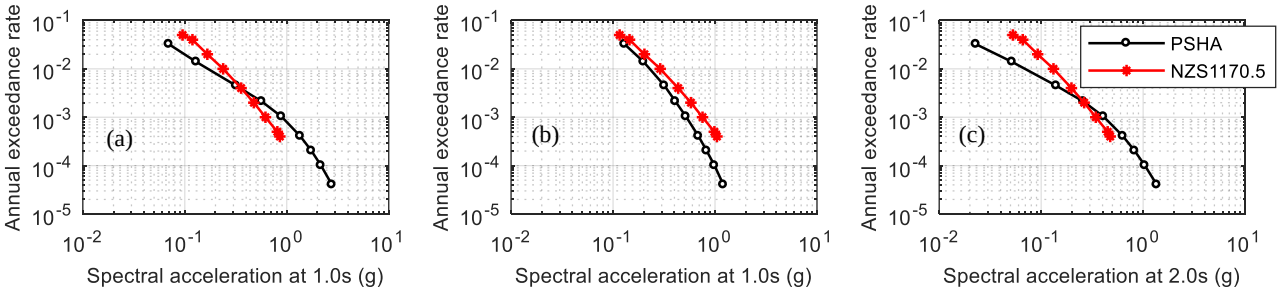


***Figure 10. Hazard curve associated with the spectral acceleration at (a) 1.0 s, Wellington; (b) 1.0 s, Christchurch; and (c) 2.0 s, Wellington***

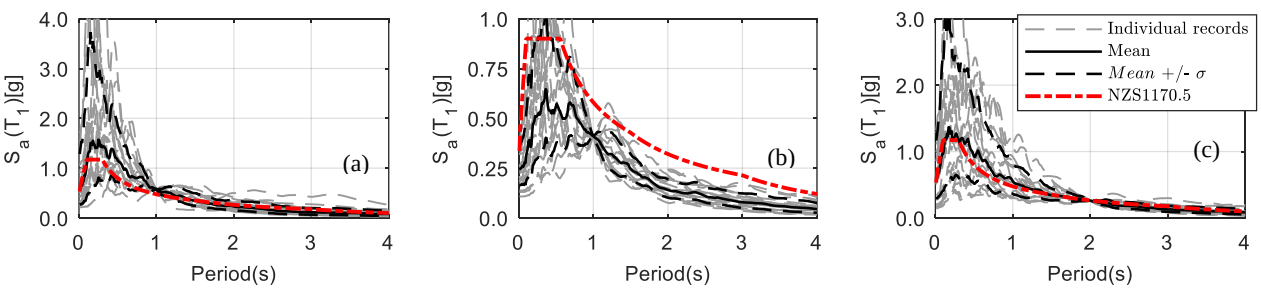


***Figure 11. Geometric mean acceleration response spectrum for (a) Wellington conditioning period of 1.0 s (b) Christchurch conditioning period of 1.0 s (c) Wellington conditioning period of 2.0 s .***

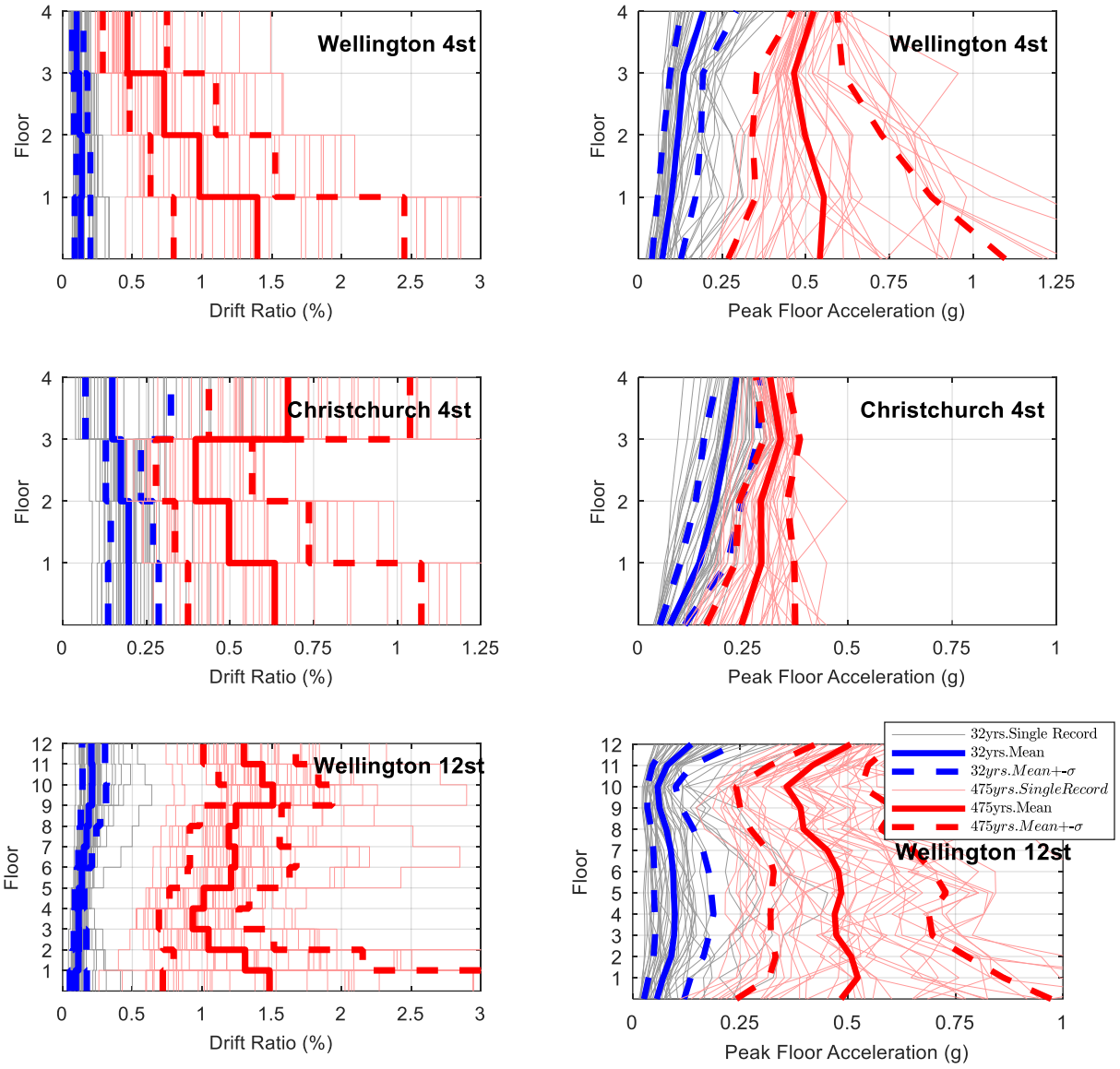


***Figure 12: Building response obtained from NLTH analyses.***

The loss results obtained following the "rigorous" [7] procedure are presented in terms of expected annual loss ratio (EAL) in Table 3. Furthermore, the loss predicted for each ground motion at each stripe in addition to the median, 16$^{th}$ and 84$^{th}$ percentiles are illustrated in Figure 13. The prediction approach has been iterated considering a replacement threshold of 0.4, as illustrated in Figure 14. It is seen that the loss curve in Figure 14 is identical as those depicted in Figure 13 for intensities with loss ratio smaller than 0.4; however, the line changes the slope (becomes sharper) and increases to 1 for ground motions with loss ratio larger than 0.4. Moreover, the loss contribution at each stripe has been computed for all three case study buildings. Figure 15 illustrates the expected annual loss contribution (as a percentage of building replacement cost) at each stripe for the three case study buildings in addition to component loss occurring at the 1$^{st}$ and 4$^{th}$ intensity levels (stripes) associated with the code serviceability and ultimate limit state design hazard levels.

The expected annual loss associated with the Wellington case study buildings presented in Table 3 is seen to be larger than that of the Christchurch case study buildings. The difference in the loss estimated for the Wellington and Christchurch case study buildings is mainly attributed to differences in hazard curves and the spectral acceleration at which each case study building has been designed and evaluated. To clarify, Figure 10 compares the spectral acceleration proposed by NZS 1170.5 (2004) and the probabilistic seismic hazard analysis results at conditioning periods of 1.0 s and 2.0 s.

***Table 3: The expected annual loss ratio (EAL) found through rigorous approach.***

| City | Wellington | | Christchurch |
|---|---|---|---|
| Case study building | 4-storey | 12-storey | 4-storey |
| Expected annual loss (%) | 0.17 | 0.15 | 0.07 |

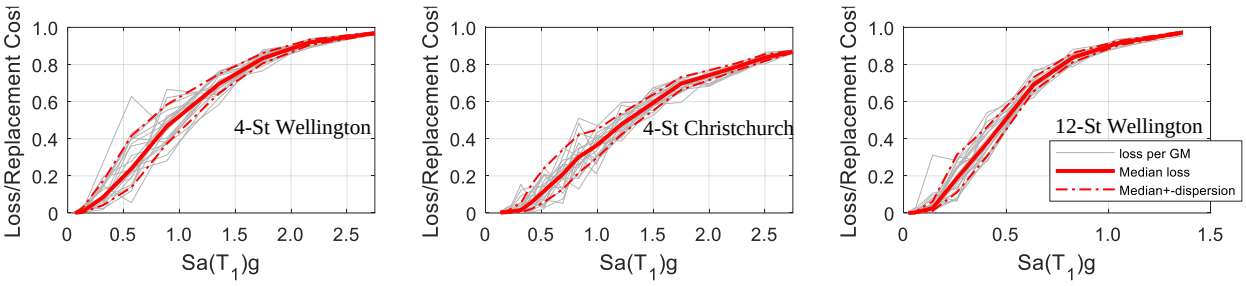


***Figure 13: Loss assessment results for each ground motion at each stripe following PEER approach.***

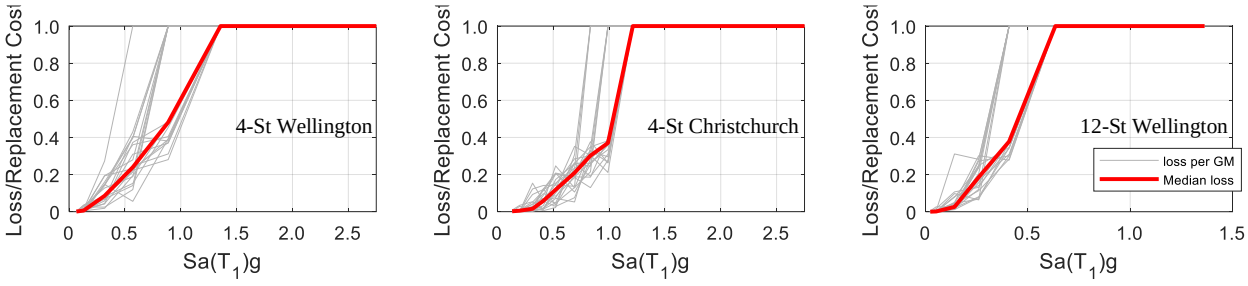


***Figure 14: Loss assessment results for each ground motion at each stripe obtained from the PEER approach and considering a loss threshold of 0.4 of building replacement value.***

Figure 10 illustrates that the Christchurch 4-storey case study building has been designed using code design intensity levels that are larger (at both SLS and ULS) than the PSHA demands at the same return periods. However, the Wellington 4- and 12-storey case studies have been designed for larger demands than the PSHA results at low intensities (SLS) and smaller demands than the PSHA results at high intensities (ULS). As is illustrated in Figure 15, the loss contribution at low intensities is consequently small for the Wellington case studies. However, the Christchurch case study shows higher loss contributions at low intensities but these are not as high when the intensity increases due to the increased difference between design and assessment intensities. Given the high loss contribution of the lowest intensity run for the Christchurch 4-storey building, a lower intensity stripe was also run but the EAL did not increase significantly.

The most fragile components at the first intensity level are seen to be partitions and ceilings as illustrated by Figure 15; this is in line with the low drift and acceleration capacity associated with the 1st damage state of partitions and ceilings, respectively. The intensity associated with damage initiation of the partitions is smaller than that which causes damage to the ceilings. Conversely, the eccentrically braced frame shear links govern the loss at the 4th intensity level (equivalent to the ultimate limit state). It is also interesting to see the large contribution that structural damage makes to the EAL. This is considered to be a result of the relatively high costs attributed to the repair of EBF links that can begin to require repairs from relatively low levels of drift demand (and therefore intensity). Indeed, the acceleration demands increase at a slower rate after reaching the yield point of the structure (around the intensity levels of 0.17 g, 0.08 g, and 0.20 g associated with Wellington 4- and 12-storey, and the Christchurch 4-storey buildings, respectively) while the drift demand keeps growing at an even larger rate post-yield as a result of the structure's stiffness degradation.

The loss disaggregation results, illustrated in Figure 15, were computed through multiplication of the intensity's rate of occurrence (i.e. the tributary interval of the rates of exceedance) and the monetary loss at that hazard level. As such, one expects to see the regeneration of a lognormal loss contribution curve. However, the curve may exhibit some discontinuity depending on the loss expected at each hazard level and the intensity exceedance rate differences between hazard levels. Furthermore, the results reflect the acceleration sensitive components' large loss contribution for EBF systems which stems from the relatively high stiffness provided by such systems, especially in the elastic range of behaviour. This high initial stiffness develops relatively large acceleration demands (with a median value of around 0.25 g) that can damage acceleration-sensitive components (such as the ceilings which had a median acceleration capacity of 0.46 g) considering the dispersion for both demand and capacity.

**Simplified Loss-Based Assessment**

The accuracy of the simplified loss-based assessment approach outlined in Sections 3 and 4 is now examined by comparing predictions with results from the previous section. As such, the simplified loss models are adopted to estimate the expected annual loss. The correct values for the parameters required to define either the two-damage or three-damage state loss models are investigated through the process illustrated previously.

*Investigation of Simplified Loss Model Parameters for Eccentrically Braced Frame Buildings*

As illustrated in Figure 6, to apply Equation 2 and Equation 3, one needs the loss ratio, intensity, and given limit states' exceedance return periods to estimate the expected annual loss. In this example, to avoid introducing uncertainty associated with the use of simplified structural analyses (recognizing that the scope of the paper is to gauge the accuracy of the simplified loss models, not the accuracy of structural analysis methods), the MSA results were used to find the intensities at which different limit states are exceeded. With regards to the loss estimation procedure, firstly, the generic floor loss functions proposed by Dhakal and Saha [26], simplified elastic peak floor acceleration provided by Haymes et al. [49], and displacement profile proposed by O'Reilly and Sullivan [56] were adopted to estimate the loss-intensity curve. Secondly, the building specific floor loss functions Ramirez and Miranda [24] and

median values of maximum drift and peak floor acceleration found from MSA were employed. The results of the two approaches in the form of the loss-intensity curves are illustrated in Figure 16 and Figure 17, respectively. Note that the loss curves shown here are the outcome of a large number of demand (IDR/PFA) assessments to better capture the shape of loss variation curves. However, in practice one could develop similar curves by examining a more limited number of loss or intensity levels.

To assess the performance of the loss assessment procedure described in Figure 7, the median drift and acceleration demands profile along height of the structure are averaged and considered as demand for all storeys. As such, the loss obtained at each intensity is taken to represent the storey loss assuming that the building value is uniformly distributed among all levels. As illustrated in Figure 18, the storey loss functions obtained through SLAT (Bradley 2009) and the procedure described in Figure 7 are compared. It is seen that the investigated storey loss slightly underestimates the storey loss obtained from SLAT. Whilst some errors in different parts of the procedure may be cancelling out the errors in other parts, the differences shown do not appear large. Nevertheless, a broader set of case study buildings could be examined to more fully explore the accuracy of the approach as part of future research.

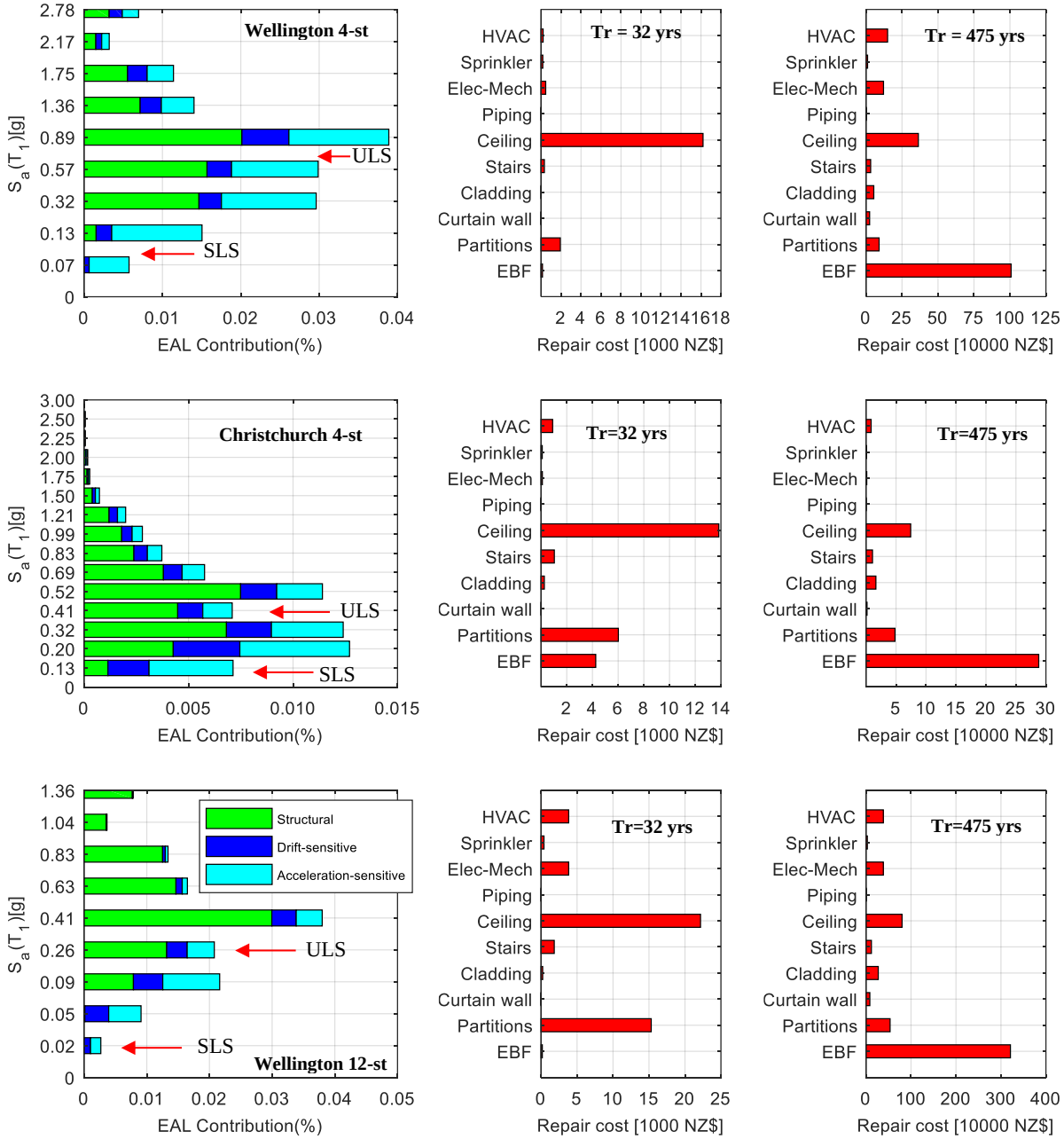


***Figure 15: Expected annual loss contributions (left) and the loss associated with different elements occurring at 1st (32 y return period which is close to the SLS design return period, middle) and 4th intensity levels (475 y return period, right) used for serviceability and ultimate limit state design.***

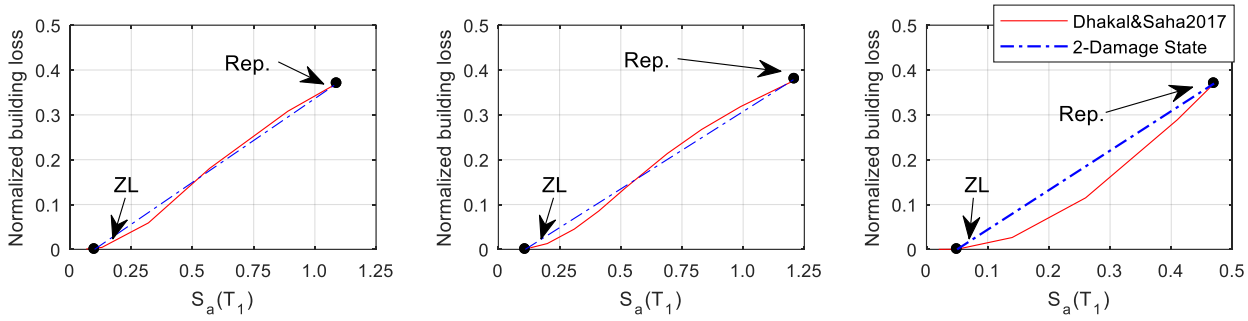


***Figure 16: Median repair costs (loss, normalized by the replacement cost) estimated for (a) Wellington 4-storey (b) Christchurch 4-storey, and (c) Wellington 12-storey buildings using the generic floor loss functions by Dhakal and Saha [26], PFA estimates according to Haymes et al. (2020) and displacement profile proposed by O'Reilly and Sullivan [48].***

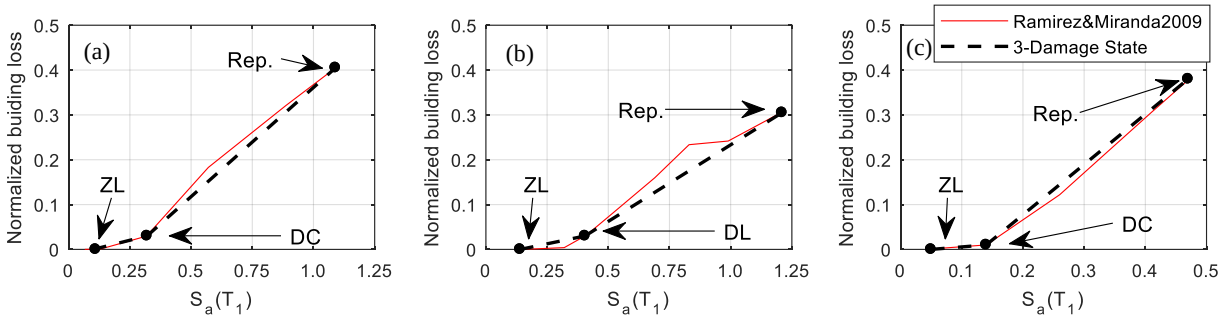


***Figure 17: Median repair costs (loss, normalized by the replacement cost) estimated for (a) Wellington 4-storey (b) Christchurch 4-storey (c) Wellington 12-storey buildings using building-specific floor loss functions (Ramirez and Miranda 2009) and IDR and PFA found from MSA.***

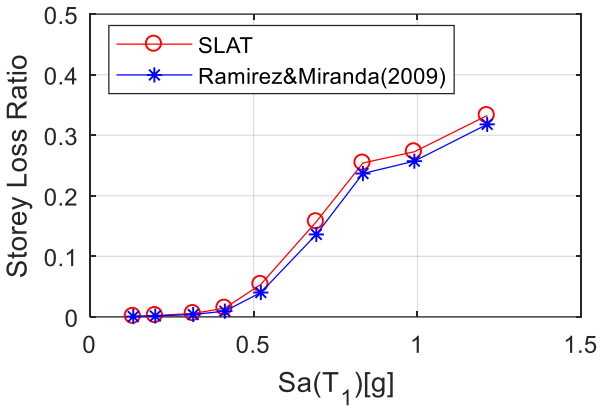


***Figure 18: Storey loss functions achieved from SLAT (Bradley 2009) and the procedure outlined in Section 5.***

It is seen from Figure 17 that the building-specific approach would suggest that the loss increases at a slow rate for low intensity levels but the rate then increases at higher intensity levels. Using the generic floor loss functions (in Figure 16) the rate of loss increase is instead predicted to be relatively constant, as illustrated in Figure 16. Subsequently, a two-damage state loss model could represent the seismic loss variations for results in Figure 16 and the three-damage state loss model could be a more suitable fit to the results illustrated in Figure 17. Note that increasing the number or dimensions of the lateral load resisting system's elements could change the slope of the loss curve across all intensities. However, the change of slope is also a function of the yield strength to weight ratio and building period, which implies that the impact of different changes on drifts and accelerations may not always be uniform. From Table 4***Table 4*** it is seen that generally the zero-loss damage state initiates at a drift of 0.17% (corresponding to the median drift capacity minus one standard deviation for DS1 of partitions) and the replacement damage state at 3%, respectively, can be applied to estimate the associated intensity measure (as illustrated in Figure 14) for use in the two-damage state loss model (Equation 2). Furthermore, the normalized loss ratios at 3% drift for the 4- and 12-storey buildings located in Wellington are 0.37 and 0.38, respectively, and 0.38 for the 4-storey building located in Christchurch, as illustrated in Figure 16. However, in these examples the replacement loss ratio is taken to be equal to 0.4 (also suggested as replacement loss threshold in [7]) for all case study buildings, as listed in Table 4 and Table 5.

As stated in Section 3, the benefit of the three-damage state loss model is the possibility of considering an extra limit state (the damage control limit state) beyond which the gradient of the loss-intensity curve is expected to increase due to specific design checks or provisions that protect most elements from damage prior to that intensity level. In New Zealand, specification of a damage-control limit state at which losses are limited to 5% of the building replacement cost is currently being considered [1]. Following the algorithm illustrated in Figure 7, the drift of the zero-loss, damage control, and replacement limit states threshold are found to be 0.17% (partitions 1$^{st}$ damage state median drift minus one standard deviation drift capacity), 0.7% (which is the minimum of the 2$^{nd}$ damage state's drift capacity of EBF links), and 3.0%, respectively, as listed in Table 5. A damage control limit state loss ratio is not defined precisely here because the current case studies were not designed for damage-control but rather followed the New Zealand standard [51] approach that considers only SLS and ULS requirements. However, it is feasible that additional damage states be incorporated in seismic design in the future, such as for low-damage design (refer to [1]). As such, the ability to allow for this in simplified loss assessment has been considered here. The damage control limit state loss ratio is set as 3% and 1% respectively for the 4- and 12-storey located in Wellington and 3% for the 4-storey located in Christchurch, since the loss curves do present a non-linear variation with intensity around these points.

*Table 4: Parameters required for simplified risk analysis adopting modified bi-linear loss model (also known as two damage state loss model) (Equation 2).*

| Case study buildings | $IDR_0$ (%) | $IM_0$ ($S_a[T_1]$) | $IDR_{Rep}$ (%) | $IM_{Rep}$ ($S_a[T_1]$) | R |
|---|---|---|---|---|---|
| **WELL4st** | 0.17 | 0.11 | 3 | 1.09 | 0.40 |
| **WELL12st** | 0.17 | 0.05 | 3 | 0.47 | 0.40 |
| **CHCH4st** | 0.17 | 0.14 | 3 | 1.21 | 0.40 |

*Table 5: Parameters required for the three damage state-loss model.*

| Building | $IDR_0$ (%) | $IM_0$ (g) | $IDR_{DC}$(%) | $IM_{DC}$ (g) | $IDR_{Rep}$(%) | $IM_{Rep}$ (g) | C | R |
|---|---|---|---|---|---|---|---|---|
| **WELL-4st** | 0.17 | 0.11 | 0.7 | 0.32 | 3.0 | 1.09 | 0.03 | 0.40 |
| **WELL-12st** | 0.17 | 0.05 | 0.7 | 0.14 | 3.0 | 0.47 | 0.01 | 0.40 |
| **CHCH-4st** | 0.17 | 0.14 | 0.7 | 0.40 | 3.0 | 1.21 | 0.03 | 0.40 |

*R and C represent the replacement and damage control point normalized loss ratio.

*Simplified Loss-Based Assessment Results*

The results from the two-damage state and three-damage state loss models, in addition to those found from rigorous [7] loss assessment, are listed in Table 6. Furthermore, the 2-DS loss model and 3-DS loss model are compared separately with the median loss estimated using the PEER approach as illustrated in Figure 19 and Figure 20, respectively. The intensity associated with the limit state's rate of exceedance obtained via the improved SAC/FEMA approach is adopted to provide a fair comparison between the two simplified and rigorous approaches. Despite the fact that simpler assumptions were made to estimate the parameter values required for the two-damage state loss model, it is evident from Table 6 that it is able to provide reasonably accurate estimation of the expected annual loss ratio. Furthermore, the three-damage state loss model provides the chance to reflect on the impact of any decisions that may be made to limit the losses that develop in the low to medium intensity range, and also the tolerable loss that permits repair of a damaged building. For further clarification, Appendix C provides hand calculations for both the 2- and 3-damage state models employed to compute the expected annual loss.

*Table 6: Comparison of expected annual loss estimates (as % of building replacement cost) obtained via the two-damage state and newly proposed three-damage state loss models, with those obtained via rigorous loss assessment with a replacement threshold loss ratio of 0.40 for all case study buildings.*

| Case study building | 4-Storey (EAL) | | 12-Storey (EAL) |
|---|---|---|---|
| | Wellington | Christchurch | Wellington |
| **Two-damage state loss model** | 0.20% | 0.12% | 0.19% |
| **Three-damage state loss model** | 0.17% | 0.07% | 0.15% |
| **Rigorous method (FEMA p58)** | 0.17% | 0.07% | 0.15% |

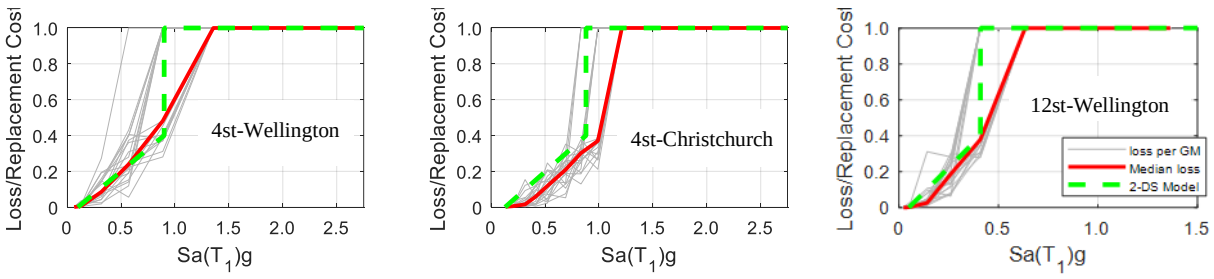


*Figure 19: Comparison of 2-DS loss model after accounting for uncertainties and median loss obtained following PEER approach.*

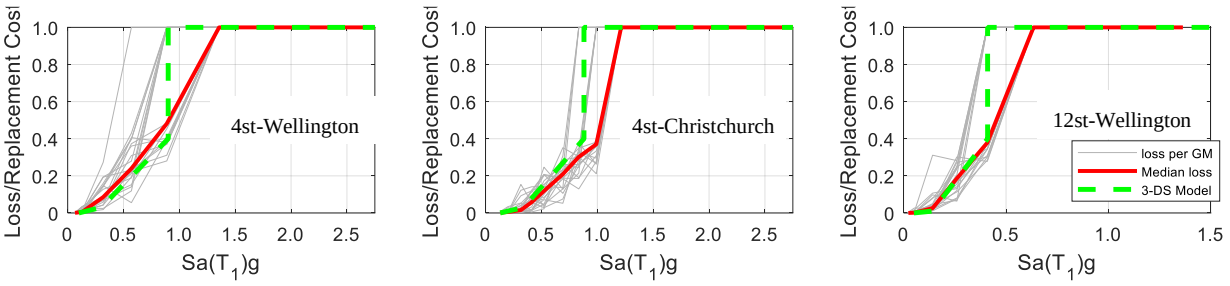


***Figure 20: Comparison of 3-DS loss model after accounting for uncertainties and median loss obtained following PEER approach.***

In Table 6, the expected annual losses obtained from the simplified approach (using strorey-based loss functions) are compared with those obtained from the rigorous method. The comparison is seen to be good and thus, this paper has successfully formulated new simplified expressions for EAL, as a function of two or three limit state loss values. Nonetheless, it should be emphasized that the accuracy of the simplified method will be somewhat dependent on the accuracy of the structural analysis method, storey based-loss functions and dispersion estimates used.

## FACTORS AFFECTING THE ACCURACY OF THE DAMAGE STATE LOSS-INTENSITY MODEL

In this section, the effect of the hazard estimation methodology and simplified loss model on the accuracy of the simplified loss estimation approach is investigated. Figure 21 illustrates the spectral acceleration hazard curve and the values obtained through fitting technique. It is seen that there is a perfect match between the hazard values and the fit curve for the whole range of acceleration intensities corresponding to the Christchurch 1.0s and the first five values associated with Wellington 1.0s and 2.0s demands. As such, applying the fit hazard curve values does not affect the accuracy of the final loss estimates significantly.

To demonstrate the potential impact of uncertainty on the expected annual loss, the three limit state loss-intensity approach was re-applied assuming the uncertainty in demand and capacity equal to zero and the results are reported in Table 7. It is seen that the EAL obtained through simplified approach ignoring the uncertainties is significantly underestimated.

The effect of the loss model on the accuracy of the simplified loss estimation approach can also be highlighted by comparing the rigorous, two-damage state, and three-damage state loss versus intensity models, as illustrated in Figure 22. As stated previously, the loss curve has been computed using median drift and peak floor acceleration demands and variability in engineering demand parameters has not been accounted for when computing the loss ratio associated with each limit state. However, the variability in drift and acceleration demands was accounted for at the 2nd stage of the simplified approach by employing the improved SAC/FEMA solution in which dispersion in demand and capacity is considered (see Equations 5 to 7). As such, the loss curve values achieved by employing the median demands are expected to appear smaller than the loss values obtained from rigorous assessment. The results in Figure 22 show that the rigorous loss curve is shifted to the left (as expected) relative to the 3-damage state model but less so for the 2-damage state model, highlighting the benefits of the 3-damage state model.

***Table 7: Comparing the expected annual losses with and without the uncertainty in demand and capacity.***

| Case study building | 4-Storey (EAL) | | 12-Storey (EAL) |
|---|---|---|---|
| | Wellington | Christchurch | Wellington |
| **Three-damage state loss model** $\boldsymbol{\beta_D = 0\ and\ \beta_C = 0}$ | 0.12% | 0.04% | 0.11% |
| **Rigorous method (FEMA p58) considering uncertainties** | 0.17% | 0.07% | 0.15% |

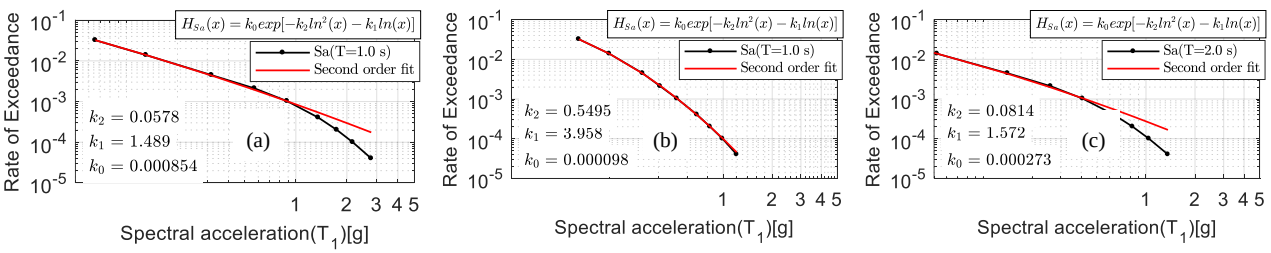


***Figure 21: Spectral acceleration at first mode (Sa(T1)[g]) hazard curve and the second order fit technique approximation (a) Wellington 1.0 s, (b) Christchurch 1.0 s, (c) Wellington 2.0 s.***

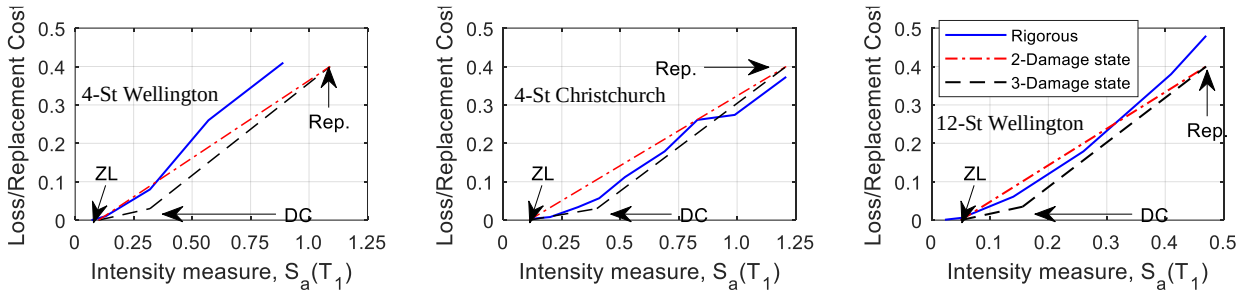


***Figure 22: Simplified two-damage state and three-damage state intensity-limit state loss model.***

***Table 8: Impact of replacement loss ratio (R) on expected annual loss (EAL) as obtained by re-running SLAT analyses with different R values.***

| Approach | WELL 4st | CHCH 4st | WELL 12st |
|---|---|---|---|
| **Rigorous method (R=0.4)** | 0.174 | 0.0694 | 0.145 |
| **Rigorous method (R=0.7)** | 0.166 | 0.0667 | 0.137 |
| **Rigorous method (R≈1.0)** | 0.155 | 0.0666 | 0.133 |

The relationships provided in this paper (Equation 2 and Equation 3) are approximate solutions for EAL calculation. Uncertainties in the four stages of the full loss assessment process are accounted for approximately in two stages. Firstly, the median loss is approximated by applying the median EDPs into damage state and consequence functions' distributions. Secondly, the annual probability of exceeding a limit state is calculated through the improved SAC/FEMA approach (Vamvatsikos 2012) in which allowances are made for uncertainties in demand and capacity and a nonlinear representation of the hazard curve is made. The IM-loss curve achieved at the end of the simplified solution and through rigorous assessment have compared well, as seen in Figure 19 and Figure 20.

The replacement loss threshold is defined to facilitate the loss calculation by setting the high intensities corresponding loss equal to building replacement value. This simplifies computations by avoiding the need to assess a collapse intensity (which would generate a loss ratio equal to 1). It also reflects the decisions that could be made by property owners with regards to the demolition of a building. Nevertheless, there is uncertainty as to the best value of a loss-threshold and the best means of accounting for uncertainties in losses around this threshold. However, the results in Table 8 show that the choice of loss threshold is actually likely to have only a limited impact on the EAL and therefore, accurate definition of this point does not appear necessary. This is understandable since generally, the intensity levels that make the highest contributions to the EAL are associated with more frequent shaking levels that do not push the structure close to the replacement threshold.

## CONCLUSIONS

To help practitioners quantify the expected annual loss (EAL) for design and assessment, a number of simplified methods have been proposed and developed. In this paper, an overview of simplified procedures has been provided and the limit-state loss versus intensity approach of Sullivan [8] has been extended in two ways. Firstly, a closed form equation for the EAL that incorporates a threshold loss value, beyond which a building is replaced, was presented. Secondly, an expression for the EAL in buildings that are better characterised with a three-damage state loss-intensity model was developed and presented.

To gauge the accuracy of the simplified loss assessment approach, it was applied to three New Zealand code compliant eccentrically braced frame buildings. The loss estimates obtained were compered against those found following the rigorous FEMA P58 methodology [7] and the simplified approach appeared to be reasonably accurate. The proposed approach was trialled here only for symmetric case study buildings, and further research is required to test its application to asymmetric buildings. The solution was developed for two cases in which the loss-intensity (considering the loss conditioned on median demand) is either idealised using two or three damage states (that would ideally be linked to design limit states). This implies that the solutions are not likely to be accurate for cases with different shaped loss-intensity curves.

The framework has been proposed for new design buildings, and as such, the best means of assessing the EAL of pre-code or deficient existing buildings should be examined as part of future research. Future research should also investigate means of relating repair cost ratios with design limit states as well as better means of accounting for uncertainties.

## ACKNOWLEDGEMENTS

This project was partially supported by QuakeCoRE, a New Zealand Tertiary Education Commission-funded Centre. This is QuakeCoRE publication number 0281. The authors gratefully acknowledge the contributions of the reviewers and editor who prompted a number of improvements to the paper, as well as to Claire Dong for her comments and suggestions.

## REFERENCES

1 Campbell P (2018). "Proposed low damage design guidance - A NZ Approach". *17th US-Japan-New Zealand Workshop on the Improvement of Structural Engineering and Resilience*, Queenstown, NZ, 8 pp. https://www.atcouncil.org/docman/atc-15-16-papers/154-p1-02-campbell/file

2 Pettinga J (2021). "Directing low-damage seismic design with building functionality". *Proceedings of the New Zealand Society for Earthquake Engineering Annual Technical Conference.* https://repo.nzsee.org.nz/handle/nzsee/2338

3 Pampanin S (2012). "Reality-check and renewed challenges in earthquake engineering: Implementing low-damage systems–from theory to practice". *Bulletin of New Zealand Society of Earthquake Engineering*, **45**(4): 137-160. https://doi.org/10.5459/bnzsee.45.4.137-160

4 Mayes R, Wetzel N, Weaver B, Tom K, Parker W, Brown A and Pietra D (2013). "Performance based design of buildings to assess damage and downtime and implement a rating system". *Bulletin of New Zealand Society for Earthquake Engineering*, **46**(1): 40-55. https://doi.org/10.5459/bnzsee.46.1.40-55

5 Daniell JE, Khazai B, Wenzel F and Vervaeck A (2013). "The CATDAT damaging earthquakes database". *Natural Hazards Earth Systems Sciences*, **11**(8): 2235-2251. https://doi.org/10.5194/nhess-11-2235-2011

6 SEAOC Vision Committee (1995). "Performance-based seismic engineering". *Structural Journal of Engineers Association of California*, California, USA.

7 FEMA (2012). "*FEMA P-58-1: Seismic Performance Assessment of Buildings Volume 1—Methodology*". Federal Emergency Management Agency and Applied Technology Council (ATC), Redwood City, CA, USA. https://femap58.atcouncil.org/

8 Sullivan T (2016). "Use of limit state loss versus intensity models for simplified estimation of expected annual loss". *Journal of Earthquake Engineering*, **20**(6): 954-974. https://doi.org/10.1080/13632469.2015.1112325

9 Calvi GM, Sullivan TJ and Welch D (2014). "A seismic performance classification framework to provide increased seismic resilience". *Perspectives on European Earthquake Engineering and Seismology*, pp. 361-400. https://link.springer.com/chapter/10.1007/978-3-319-07118-3_11

10 Fajfar P and Dolšek M (2012). "A practice-oriented estimation of the failure probability of building structures". *Earthquake Engineering and Structural Dynamics*, **41**(3): 531-547. https://doi.org/10.1002/eqe.1143

11 Sullivan TJ, Welch DP and Calvi GM (2014). "Simplified seismic performance assessment and implications for seismic design". *Earthquake Engineering and Engineering Vibration*, **13**(1): 95-122. https://doi.org/10.1007/s11803-014-0242-0

12 Hwang SH and Lignos DG (2017). "Earthquake-induced loss assessment of steel frame buildings with special moment frames designed in highly seismic regions". *Earthquake Engineering and Structural Dynamics*, **46**(13): 2141-2162. https://doi.org/10.1002/eqe.2898

13 Orumiyehei A and Sullivan TJ (2021). "Quantifying the likelihood of exceeding a limit state via the displacement-based assessment approach". *Journal of Earthquake Engineering*, **26**(8): 4346-4364. https://doi.org/10.1080/13632469.2020.1828200

14 Orumiyehei A and Sullivan TJ (2021). "Displacement-based seismic assessment of the likelihood of failure of reinforced concrete wall buildings". *Buildings*, **11**(7): 295. https://doi.org/10.3390/buildings11070295

15 Porter KA, Beck JL and Shaikhutdinov RV (2002). "Sensitivity of building loss estimates to major uncertain variables". *Earthquake Spectra*, **18**(4): 719-743. https://doi.org/10.1193/1.151

16 Luco N and Cornell CA (1998). "Effects of random connection fractures on the demands and reliability for a 3-story pre-Northridge SMRF structure". *Proceedings of the 6th US National Conference on Earthquake Engineering*, **244**: 1-12.

17 O'Reilly GJ and Sullivan TJ (2017). "Quantification of modelling uncertainty in existing Italian RC frames". *Earthquake Engineering and Structural Dynamics*, **47**(4): 1054-1074. https://doi.org/10.1002/eqe.3005

18 Gentile R, Galasso C and Pampanin S (2021). "Material property uncertainties versus joint structural detailing: Relative effect on the seismic fragility of reinforced concrete frames". *Journal of Structural Engineering*, **147**(4): 04021007. https://orcid.org/0000-0002-7682-4490

19 Haselton CB, Goulet CA, Mitrani-Reiser J, Beck JL, Deierlein GG, Porter KA, Stewart JP and Taciroglu E (2008). "*An assessment to benchmark the seismic performance of a code-conforming reinforced-concrete moment-frame building*". Pacific Earthquake Engineering Research Center. https://authors.library.caltech.edu/33801/1/web_PEER712_HASELTONetal.pdf

20 Kazantzi A, Vamvatsikos D and Lignos D (2014). "Seismic performance of a steel moment-resisting frame subject to strength and ductility uncertainty". *Journal of Engineering Structures*, **78**: p. 69-77. https://doi.org/10.1016/j.engstruct.2014.06.044

21 Farag M, Mehanny S, Kohrangi M, Vamvatsikos D and Bakhoum M (2019). "Precast beam bridges with a buffer–gap–elastomeric bearings system: Uncertainty in design parameters and randomness in ground records". *Journal of Bridge Engineering*, **24**(5): 04019034. https://doi.org/10.1061/(ASCE)BE.1943-5592.0001396

22 Fox MJ and Sullivan TJ (2016). "Use of the conditional spectrum to incorporate record-to-record variability in simplified seismic assessment of RC wall buildings". *Earthquake Engineering and Structural Dynamics*, **45**(3): 463-482. https://doi.org/10.1002/eqe.2669

23 Baker JW (2010). "Conditional mean spectrum: Tool for ground-motion selection". *Journal of Structural Engineering*, **137**(3): 322-331. http://dx.doi.org/10.1061/(ASCE)ST.1943-541X.0000215

24 Ramirez CM and Miranda E (2009). "*Building-specific loss estimation methods and tools for simplified performance-based earthquake engineering*". Stanford University. Report No. 171. https://stacks.stanford.edu/file/druid:zy329mj7285/TR171_Ramirez.pdf

25 Welch DP, Sullivan TJ and Calvi GM (2012). "*Developing direct displacement-based design and assessment procedures for performance-based earthquake engineering*". IUSS Press. Pavia, Italy. https://doi.org/10.1080/13632469.2013.851046

26 Dhakal RP and Saha S (2017). "Loss optimization seismic design (LOSD): Beyond seismic loss assessment". *Proceedings of 16th World Conference on Earthquake Engineering*, Santiago, Chile. https://www.wcee.nicee.org/wcee/article/16WCEE/WCEE2017-163.pdf

27 Khakurel S, Dhakal RP, Yeow TZ and Saha S (2020). "Performance group weighting factors for rapid seismic loss estimation of buildings of different usage". *Earthquake Spectra*, **36**(3): 1141-1165. https://doi.org/10.1177/8755293019901311

28 Shahnazaryan D, O'Reilly GJ and Monteiro R (2021). "Story loss functions for seismic design and assessment: Development of tools and application". *Earthquake Spectra*, **37**(4). https://doi.org/10.1177/87552930211023523

29 O'Reilly GJ and Calvi GM (2021). "A seismic risk classification framework for non-structural elements". *Bulletin of Earthquake Engineering*, **19**: 5471–5494. https://doi.org/10.1007/s10518-021-01177-y

30 Standards NZ (2004). "*NZS 1170.5: Structural Design Actions Part 5: Earthquake Actions–New Zealand*". Standards New Zealand, Wellington, NZ.

31 Turner CWO, Spooner B and Hanson FMH (2003). *Bridge Manual*. Transit New Zealand, Wellington, NZ.

32 Sullivan T, Priestley N and Calvi GM (2012). *A Model Code for the Displacement-Based Seismic Design of Structures, DBD12*. IUSS Press, Pavia, Italy.

33 Welch D, Sullivan T and Calvi G (2014). "Developing direct displacement-based procedures for simplified loss assessment in performance-based earthquake engineering". *Journal of Earthquake Engineering*, **18**(2): 290-322. https://doi.org/10.1080/13632469.2013.851046

34 Sullivan TJ and Calvi GM (2013), "*Developments in the Field of Displacement-Based Seismic Assessment*". EUCENTRE, Pavia, Italy.

35 Formisano A, Vaiano G and Fabbrocino F (2019). "A seismic-energetic-economic combined procedure for retrofitting residential buildings: A case study in the province of Avellino (Italy)". *AIP Conference Proceedings*. https://doi.org/10.1063/1.5114435

36 Cardone D, Sullivan T, Gesualdi G and Perrone G (2017). "Simplified estimation of the expected annual loss of reinforced concrete buildings". *Earthquake Engineering and Structural Dynamics*, **46**(12): 2009-2032. https://doi.org/10.1002/eqe.2893

37 Krawinkler H, Zareian F, Medina R and Ibarra L (2006). "Decision support for conceptual performance-based design". **35**(1): 115-133. https://doi.org/10.1002/eqe.536

38 Elwood K, Marquis F and Kim J (2015). "Post-earthquake assessment and reparability of RC buildings: Lessons from Canterbury and emerging challenges". *Proceedings of the Tenth Pacific Conference on Earthquake Engineering: Building an Earthquake-Resilient Pacific*.

39 FEMA (2012). "*FEMA P58-2: Seismic Performance Assessment of Buildings: Volume 2 (Implementation)*". Applied Technology Council, Redwood City, CA.

40 O'Reilly GJ and Calvi GM (2019). "Conceptual seismic design in performance-based earthquake engineering". *Journal of Earthquake Engineering and Structural Dynamics*, **48**(4): 389-411. https://doi.org/10.1002/eqe.3141

41 Shahnazaryan D and O'Reilly GJ (2021). "Integrating expected loss and collapse risk in performance-based seismic design of structures". *Bulletin of Earthquake Engineering*, **19**(2): 987-1025. https://doi.org/10.1007/s10518-020-01003-x

42 Retamales R, Davies R, Mosqueda G and Filiatrault A (2013). "Experimental seismic fragility of cold-formed steel framed gypsum partition walls". *Journal of Structural Engineering*, **139**(8): 1285-1293. https://doi.org/10.1061/(ASCE)ST.1943-541X.0000657

43 ASCE (2014). "*ASCE 41-13: Seismic Evaluation and Retrofit Rehabilitation of Existing Buildings*". American Society for Civil Engineers, USA.

44 Porter KA and Beck JL (2004). "Simplified PBEE to estimate economic seismic risk for buildings". *Proceedings of the International Workshop on Performance-Based Seismic Design*, Pacific Earthquake Engineering Research Center, USA.

45 Cornell CA, Jalayer F, Hamburger R and Foutch D (2002). "Probabilistic basis for 2000 SAC federal emergency management agency steel moment frame guidelines". *Journal of Structural Engineering*, **128**(4): 526-533. https://doi.org/10.1061/(ASCE)0733-9445(2002)128:4(526)

46 Vamvatsikos D (2012). "Accurate application and second-order improvement of SAC/FEMA probabilistic formats for seismic performance assessment". *Journal of Structural Engineering*, **140**(2). https://doi.org/10.1061/(ASCE)ST.1943-541X.0000774

47 Bakalis K and Vamvatsikos D (2018). "Seismic fragility functions via nonlinear response history analysis". *Journal of Structural Engineering*, **144**(10). https://doi.org/10.1061/(ASCE)ST.1943-541X.0002141

48 O'Reilly GJ and Sullivan TJ (2016). "Direct displacement-based seismic design of eccentrically braced steel frames". *Journal of Earthquake Engineering*, **20**(2): 243-278.

49 Haymes K, Sullivan T and Chandramohan R (2020). "A practice-oriented method for estimating elastic floor response spectra". *Bulletin of New Zealand Society for Earthquake Engineering*, **53**(3): 116-136. https://doi.org/10.5459/bnzsee.53.3.116-136

50 Standards NZ (2002). "*NZS 1170.0: Structural Design Actions, Part 0: General Principles*". Standards New Zealand, Wellington, NZ.

51 Standards NZ (2007). "*NZS 3404: Steel Structures Standard- New Zealand*". Standards New Zealand, Wellington, NZ.

52 Wilson EL and Habibullah A (2000). *Structural Analysis Program SAP2000*. Berkeley, California, USA.

53 Standards NZ (2002) "*NZS 1170.2: Structural Design Actions, Part 2: Wind Actions*". Standards New Zealand, Wellington, NZ.

54 Mazzoni S and McKen F (2006). "*The Open System for Earthquake Engineering Simulation (OpenSEES) User Command-Language Manual*".

55 De Francesco G and Sullivan TJ (2020). "Formulation of localized damping models for large displacement analysis of single-degree-of-freedom inelastic systems". *Journal of Earthquake Engineering*, **26**(8): 4235-4258. https://doi.org/10.1080/13632469.2020.1826370

56 O'Reilly GJ and Sullivan TJ (2016). "Direct displacement-based seismic design of eccentrically braced steel frames". *Journal of Earthquake Engineering*, **20**(2): 243-278. https://doi.org/10.1007/s10518-013-9486-8

57 Kanvinde A, Marshal K, Grilli D and Bomba G (2014). "Forensic analysis of link fractures in eccentrically braced frames during the February 2011 Christchurch earthquake: Testing and simulation". *Journal of Structural Engineering*, **141**(5). https://doi.org/10.1061/(ASCE)ST.1943-541X.0001043

58 Nascimbene R, Rassati G and Wijesundara K (2012). "Numerical simulation of gusset plate connections with rectangular hollow section shape brace under quasi-static cyclic loading". *Journal of Constructional Steel Research*, **70**: 177-189. https://doi.org/10.1016/j.jcsr.2011.09.010

59 Jalayer F and Cornell C (2009). "Alternative non-linear demand estimation methods for probability-based seismic assessments". *Earthquake Engineering and Structural Dynamics*, **38**(8): 951-972. https://doi.org/10.1002/eqe.876

60 Yeow T, Orumiyehei A, Sullivan T, MacRae G, Clifton C and Elwood K (2018). "Seismic performance of steel friction connections considering direct-repair costs". *Bulletin of Earthquake Engineering*, **16**: 5963-5993. https://doi.org/10.1007/s10518-018-0421-x

61 Bradley BA (2010). "A generalized conditional intensity measure approach and holistic ground-motion selection". *Earthquake Engineering and Structural Dynamics*, **39**(12): 1321-1342. https://doi.org/10.1002/eqe.995

62 O'Reilly GJ and Sullivan TJ (2016). "Fragility functions for eccentrically braced steel frame structures". *Engineering and Structures*, **10**(2): 367-388. https://doi.org/10.12989/eas.2016.10.2.367

63 Sullivan TJ, Fox M, Keen J and Goebbels S (2021). "Repair methods and costs for earthquake-damaged building components in New Zealand". DesignSafe-CI. https://doi.org/10.17603/ds2-c9kw-n302

## APPENDIX A

In this appendix, the approach followed to derive the two-damage state and three-damage state loss-intensity relationships, provided by Equation (2) and Equation (3) are elaborated. The two damage state loss model is composed of two parts; the first part shows the linear variation of loss as a function of intensity which begins from ZL limit state exceedance's intensity to the replacement threshold limit state's exceedance intensity. The loss ratio is assumed equal to 1 at intensities larger than replacement threshold exceedance's intensity as indicated by the second part of the two-damage state loss model. The three-damage state loss model, however, is composed of three lines: the first line communicates the loss incurring at intensities larger than ZL limit state capacity intensity and before exceeding the damage control limit state. The second line provides information regarding the loss after exceeding damage control limit state and before reaching the replacement threshold limit state. The third line presents a constant loss ratio (equal to 1) for intensities larger than replacement threshold's capacity intensity by which the building's demolition and replacement is alerted.

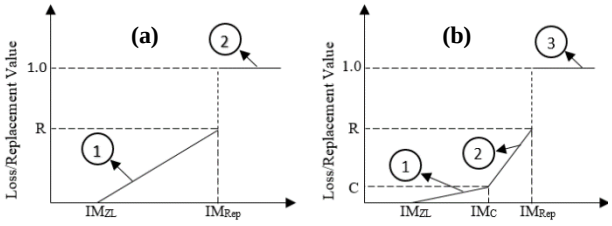


***Figure A.1: Idealised (a) two-damage state and (b) three-damage state loss-intensity (median repair cost) curves incorporating a threshold replacement limit state (before accounting for the uncertainties in demands).***

In order to obtain the expected annual loss, one shall solve the integration illustrated in Equation (A1). In the following, firstly, the steps required for achieving two damage state loss-intensity relationship demonstrated, and then the procedure which shall be followed to obtain three damage state loss-intensity model is discussed.

$$EAL = \int E[loss|IM]|d\lambda(IM)| \tag{A1}$$

where $E[loss|IM]$ is the expected monetary loss incurring at a given limit state exceedance's intensity $(IM)$, $\lambda(IM)$ is the annual frequency of exceeding a given limit state illustrated in Equation (A2), and $d\lambda(IM)$ is the derivative of the limit state hazard at the corresponding intensity.

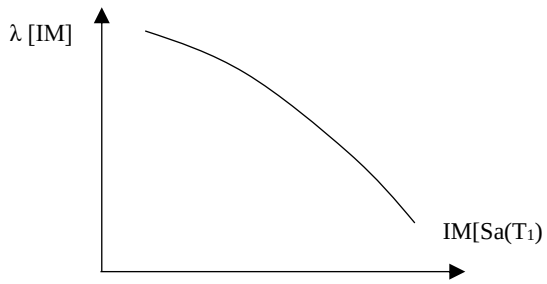


***Figure A.2: Limit state hazard curve.***

Equation (A2) initially proposed by Cornell et al. [45] for intensity measure hazard approximation. However, it is applied herein to estimate the rate of a specific LS exceedance given an intensity.

$$\lambda[LS = ls_i|IM] = k_0 \cdot IM^{-k} \tag{A2}$$

where $\lambda[LS(IM)]$ is the approximation of limit state hazard, $k_0$ and $k$ are the corresponding coefficients at the given intensity measure. The limit state hazard can also be approximated by following the framework proposed by Vamvatsikos [46] adopting a second order fit technique in log-space, as explained previously in the paper.

The idealized linear loss ratio variation as a function of intensity, illustrated in Figure A.1, can be presented by Equations (A3) and (A4).

$$LR = m_1 \cdot IM + b; \quad IM_{ZL} \leq IM \leq IM_{Rep} \tag{A3}$$

$$LR = 1; \quad IM > IM_{Rep} \tag{A4}$$

where $LR$ is the loss ratio, $m_1$ and $b$ are the slope and $y$ axis intercept, respectively, in Figure A.1; $IM_{ZL}$ is the zero loss limit state exceedance's intensity and $IM_{Rep}$ is the replacement threshold limit state exceedance's intensity. Note that from geometry the slope $(m_1)$ and y intercept $(b)$ can be obtained as illustrated in Equation (A5) and (A6), respectively.

$$m_1 = \frac{R}{(IM_{Rep} - IM_{ZL})} \tag{A5}$$

$$b = -\frac{R\ IM_{ZL}}{IM_{Rep} - IM_{ZL}} \tag{A6}$$

The expected annual loss can be computed by convolution of loss function and limit state hazard curve, as illustrated in Equation (A7).

$$EAL = \int_{\lambda_{Rep}}^{\lambda_{ZL}} (m_1(IM) + b)d\lambda + \int_0^{\lambda_{Rep}} 1 d\lambda \tag{A7}$$

where all parameters have been defined previously.

Assuming the power law function between the limit state exceedance equivalent intensity and the corresponding rate of exceedance $(\lambda)$ shown in Equation (A2), the limit state's intensity can be stated as a function of that limit state annual frequency of exceedance as illustrated in Equation (A8).

$$IM(LS = ls_i) = \left(\frac{\lambda[LS = ls_i]}{k_0}\right)^{-1/k} \tag{A8}$$

where all parameters have been defined previously.

The expected annual loss integration can be conducted by substituting Equation (A5), Equation (A6), and Equation (A8) in Equation (A7); the achieved relationship is illustrated in Equation (A9).

$$EAL = [\frac{km_1{k_0}^{1/k}}{k-1}\lambda^{\frac{k-1}{k}} + b]_{\lambda_{Rep}}^{\lambda_{ZL}} + \lambda_{Rep} \quad \text{(A9)}$$

where $\lambda_{ZL}$ and $\lambda_{Rep}$ are the annual probability of exceeding zero loss limit state and replacement threshold limit state, respectively; the other parameters have been defined previously.

Furthermore, the exponent of power law function ($k$), illustrated in Equation (A2), can be stated as illustrated in Equation (A10).

$$k = \frac{\ln(\frac{\lambda_c}{\lambda_{rep}})}{\ln(\frac{IM_c}{IM_{Rep}})} \quad \text{(A10)}$$

where $IM_c$ and $\lambda_c$ are the intensity and annual rate of exceedance, respectively, and the other parameters have been defined previously.

The relationship for expected annual loss (EAL) calculation can be achieved by substituting Equation (A10) in Equation (A9) as illustrated in Equation (A11).

$$EAL = R\frac{\left(\lambda_{ZL} - \frac{IM_{Rep}}{IM_{zl}}\lambda_{Rep}\right)}{\left(\frac{IM_{Rep}}{IM_{zl}} - 1\right)\left(1 - \frac{\ln\left(\frac{IM_{Rep}}{IM_{zl}}\right)}{\ln\left(\frac{\lambda_{zl}}{\lambda_{Rep}}\right)}\right)} - R\frac{\lambda_{zl} - \lambda_{Rep}}{\frac{IM_{Rep}}{IM_{zl}} - 1} + \lambda_{Rep} \quad \text{(A11)}$$

Note that by substituting $\lambda = 1/T$ in Equation (A11), Equation (2) provided earlier in the paper can be achieved. For three-damage state loss model the idealized linear loss ratio variation as a function of limit state exceedance's equivalent intensity (illustrated in Figure A.1) can be presented by Equations (A12), (A13), and (A14).

$$LR = m_1(IM) + b; \quad IM_{ZL} \le IM \le IM_{DC} \quad \text{(A12)}$$

$$LR = m_2(IM) + d; \quad IM_{DC} < IM \le IM_{Rep} \quad \text{(A13)}$$

$$LR = 1; \quad IM > IM_{Rep} \quad \text{(A14)}$$

where $LR$ is the loss ratio, $m_1$ and $b$ are the slope and intersection point with $y$ axis associate with the first linear function, and $m_2$ and $d$ are the slope and intersection with $y$ axis corresponding to the second linear function illustrated in Figure A.1; $IM_{ZL}$ is the zero loss limit state's intensity, $IM_{DC}$ is the damage control limit state's intensity, and $IM_{Rep}$ is the replacement threshold limit state's intensity.

$$m_1 = \frac{C}{IM_{DC} - IM_{ZL}} \quad \text{(A15)}$$

$$b = \frac{c\ IM_{ZL}}{IM_{DC} - IM_{ZL}} \quad \text{(A16)}$$

$$m_2 = \frac{R - c}{IM_{Rep} - IM_{DC}} \quad \text{(A17)}$$

$$d = \frac{(R - c)IM_{DC}}{IM_{Rep} - IM_{DC}} - c \quad \text{(A18)}$$

The expected annual loss can be computed by convolution of loss function and the limit state hazard curve, as illustrated in Equation (A19).

$$EAL = \int_{\lambda_{DC}}^{\lambda_{ZL}} (m_1(IM) + b)d\lambda + \int_{\lambda_{Rep}}^{\lambda_{DC}} (m_2(IM) + d)d\lambda + \int_0^{\lambda_{Rep}} 1d\lambda \quad \text{(A19)}$$

where all parameters have been defined previously.

The integration presented in Equation (A19) can be solved by substituting IM from Equation (A8) into Equation (A19) and conducting the integration; the outcome of this process is illustrated in Equation (A20).

$$EAL = [\frac{km_1{k_0}^{1/k}}{k-1}\lambda^{\frac{k-1}{k}} + b]_{\lambda_{DC}}^{\lambda_{ZL}} + [\frac{km_2k_0^{\frac{1}{k}}}{k-1}\lambda^{\frac{k-1}{k}} + d]_{\lambda_{Rep}}^{\lambda_{DC}} + \lambda_{Rep} \quad \text{(A20)}$$

Furthermore, the parameters $m_1$, $b$, $m_2$ and $d$ can be found as a function of loss ratio and intensity by using the geometry of linear functions, as illustrated previously in Equation (15), Equation (16), Equation (17), and Equation (18), respectively. As such, the expected annual loss (EAL) can be presented as illustrated in Equation (A21) by substituting the aforementioned parameters in Equation (A20).

$$EAL = c\frac{\left(\lambda_0 - \frac{im_{DC}}{im_{zl}}\lambda_{DC}\right)}{\left(\frac{im_{DC}}{im_{zl}} - 1\right)\left(1 - \frac{\ln\left(\frac{im_{DC}}{im_{zl}}\right)}{\ln\left(\frac{\lambda_{zl}}{\lambda_{DC}}\right)}\right)} - c\frac{\lambda_{zl} - \lambda_{DC}}{\frac{im_{DC}}{im_{zl}} - 1} + (R - c)\frac{\left(\lambda_{DC} - \frac{im_r}{im_{DC}}\lambda_r\right)}{\left(\frac{im_r}{im_{DC}} - 1\right)\left(1 - \frac{\ln\left(\frac{im_r}{im_{DC}}\right)}{\ln\left(\frac{\lambda_{DC}}{\lambda_r}\right)}\right)} - \left(\frac{R - c}{\frac{im_r}{im_{DC}} - 1} + c\right)(\lambda_r - \lambda_{DC}) + \lambda_r \quad \text{(A21)}$$

## APPENDIX B

In this Appendix as an example, the procedure for designing the Christchurch 4-storey eccentrically braced frame (EBF) steel structure is elaborated. Note that the design process of this building follows what is thought to be local design practice. In case of debatable decisions among practitioners, the aim has been to take the most direct interpretation of the standard clauses. The design process followed the New Zealand Standards for general principles (NZS 1170.0 [50]), permanent and imposed loads (NZS 1170.1 ), wind (NZS 1170.2 [53]), earthquake loading (NZS 1170.5 [30]), and steel structure design standard (NZS 3404 [51]).

The main assumptions follow:

1- The generic site is in Christchurch, soil type is D, and the near field factors are not considered.

2- Ductility factor is taken equal 3.

3- The slab stiffness contribution is negligible.

### Eccentrically Braced Frame Design Procedure

#### *Loading Details*

Based on the acquired data from the case study buildings' drawings the following non-structural elements have been considered to calculate the permanent loads (see Table B.1). Moreover, the permanent load associated with the structural elements such as beams, columns, and braces have also been accounted for (see Table B.2) in the finite element model developed in the SAP.

***Table B.1: Loading detail corresponding to non-structural elements.***

| Category | | Calculated area-distributed weight (kPa) | Rounded area-distributed weight (kPa) |
|---|---|---|---|
| **Services** | | 0.21 | 0.25 |
| **Ceilings and finishes** | | 0.42 | 0.50 |
| **Partitions** | | 0.52 | 0.50 |
| **ComFlor with secondary beams** | | 2.97 | 3.00 |
| **Roof** | | 1.00 | 1.00 |
| **Total** | Floors 1-3 | 4.12 | 4.25 |
| | Roof | 4.60 | 4.75 |

***Table B.2: Permanent loads corresponding to façade.***

| Category | Floor level | Face-distributed weight (kPa) | Linear-distributed weight (kN/m) |
|---|---|---|---|
| **Curtain wall** | 1-3 | 0.6 | 2.16 |
| | Roof | | 1.08 |
| **Precast panels (100 mm thick)** | 1-3 | 1.8 | 6.48 |
| | Roof | | 3.24 |

In the current design scenario, the perimeter frames are assumed to be sufficient to resist the earthquake loads. As such, similar frames have been placed in two horizontal directions at each side of the building, as illustrated in Figure B.1.

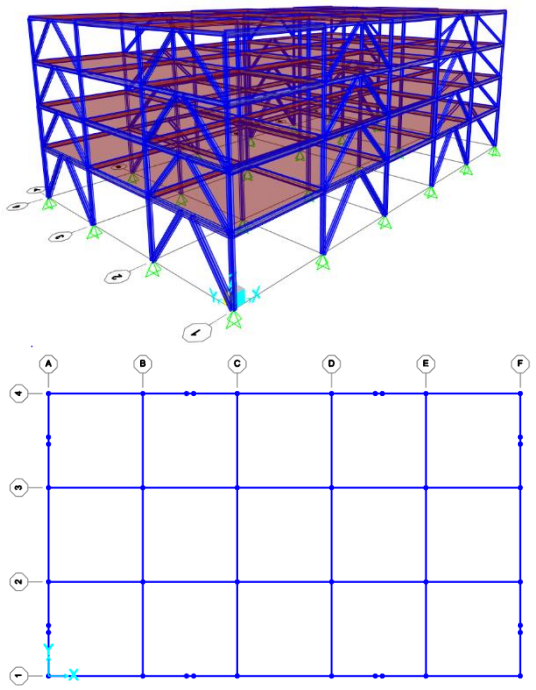


***Figure B.1: 3D representation of EBF model in SAP (left), and plan view of braced bays (right).***

Based on the above quantities, the finite element model has been adopted and a modal analysis carried out. The obtained values for the period of vibration and effective cumulative mass participation ratios are listed in Table B.3.

***Table B.3: Modal analysis results.***

| Mode | T(s) | CMP(x) | CMP(y) | CMP(T) |
|---|---|---|---|---|
| **1st X** | 0.61 | 0.85 | 0.00 | 0.00 |
| **1st Y** | 0.61 | 0.85 | 0.85 | 0.00 |
| **Torsion** | 0.38 | 0.85 | 0.85 | 0.85 |
| **2nd X** | 0.24 | 0.97 | 0.85 | 0.85 |
| **2nd Y** | 0.24 | 0.97 | 0.97 | 0.85 |

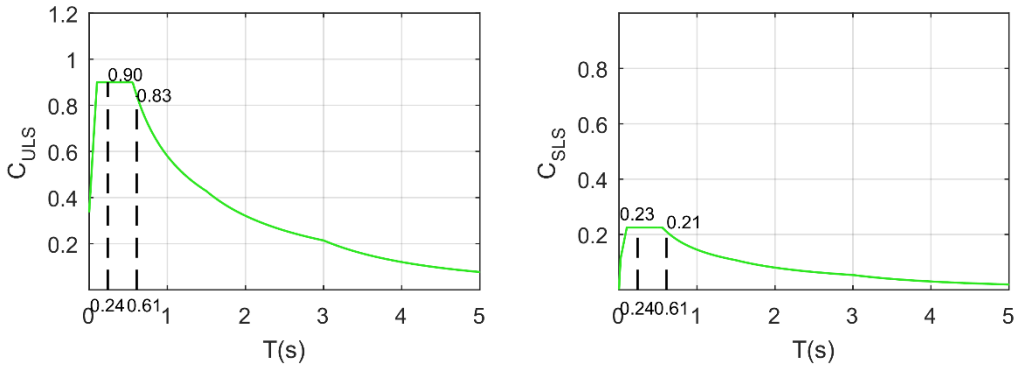


***Figure B.2: Elastic site spectrum (a) ULS (b) SLS.***

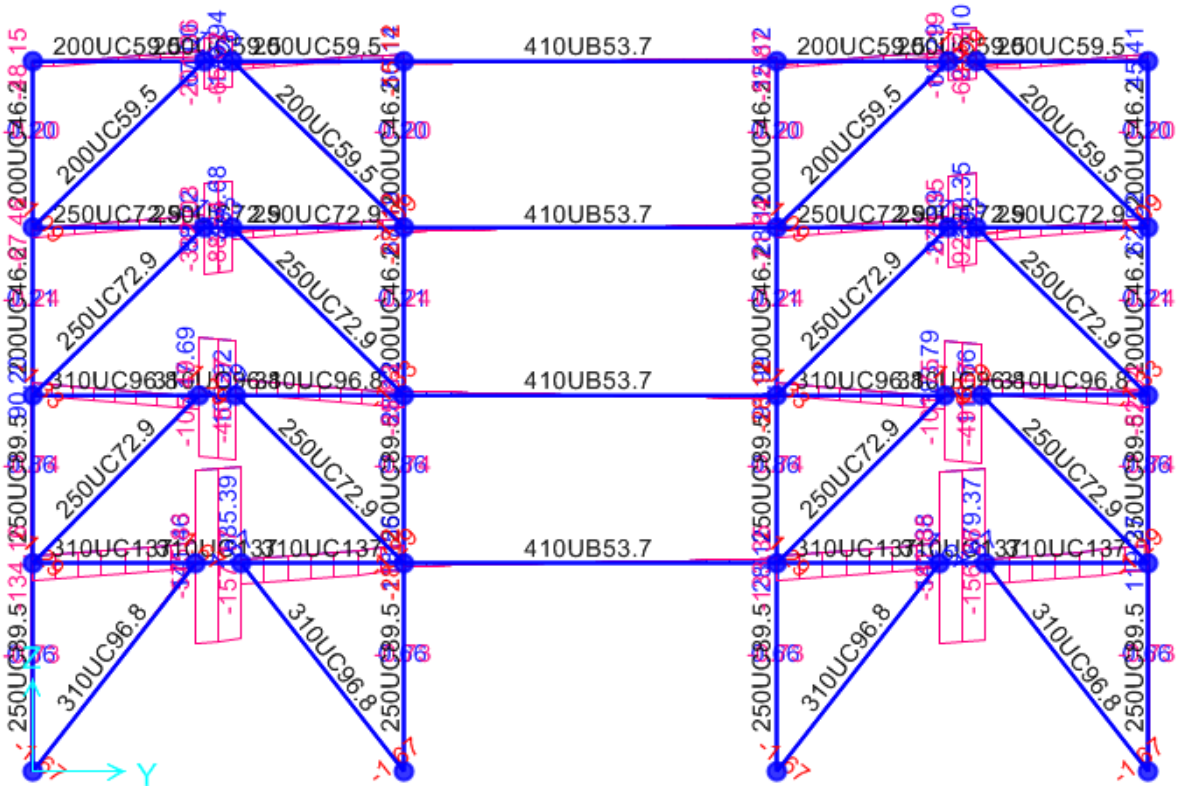


***Figure B.3: Shear demand forces in active links and collector beam.***

The response spectrum analysis was conducted using the acceleration response spectrum illustrated in Figure B.2. The active link was designed to yield, and the other components were designed based on the demands derived from simultaneous yielding of all active links along height of the building, accounting for over-strength and higher mode effects. Table B.4 illustrates the design parameters, and Table B.5 lists the base shear found from response spectrum analysis ($V^*_{RSA}$) and compares with that found from equivalent static analysis ($V^*_{ESA}$). Furthermore, Figure B.3 shows the distribution of shear force demand along each bay as well as height of the frame.

***Table B.4: Design parameters for eccentric braced frame system.***

| N(T,D) | R | Z | $S_p$ | μ | $K_\mu$ |
|---|---|---|---|---|---|
| **1** | 1 | 0.3 | 0.7 | 3 | 2.8 |

***Table B.5: RSA and ESA base shear comparison (KN).***

| Load Com. | Vx | Vy | $V^*_{ESA}$ | (80%)$V^*_{ESA}$ |
|---|---|---|---|---|
| G+0.3Q+Spec.x+Ecc.x. | 4354 | 0.00 | 4826 | 3861 |
| G+0.3Q+Spec.y+Ecc.y. | 0.00 | 4354 | 4826 | 3861 |

*RSA: Response Spectrum Analysis; ESA: Equivalent Static Analysis

As per NZS 1170.5 and NZS 3404.1, the strength and deformation demands were satisfied. The maximum active links rotation demands was 0.05 radian which found to be less than 0.08 as the code rotation limit.

For clarification, a sample of calculation will be presented herein. To make the active link dissipates energy in shear mechanism, NZS 3404 (2007) recommends a length smaller than what illustrated in Equation (B1).

$$e \leq \frac{1.6 \times M_{sx}}{V_w} \quad \text{(B1)}$$

To design the last floor active link, a universal column is considered:

$$V_{ie} = 235 \text{ kN}$$

$$200UC59.5 \rightarrow \varphi V_w = 380 \text{ kN}$$

After designing the active links, the rest of the frame components have been designed following the capacity design procedure. As such it is essential to find the maximum demands that each component would resist. Hence, in accordance with NZS 3404 Clause 12.3.3.4, the maximum over-strength factor was calculated. For that purpose, the ratio between the over-strength of the active link section and shear demand found from the analysis is calculated.

$$\varphi_0 = \frac{(\frac{380}{0.9}) \times 1.4}{235} = 2.51$$

The maximum force for a category 1 members is calculated applying $\mu$=1.25 and $S_p$ = 0.7:

$$\varphi_{e,max} = \frac{k_{\mu=3}}{k_{\mu=1.25}} = \frac{2.8}{1.25} = 2.24$$

Note that only for the design of the last floor active link, $\varphi_0$ is bigger than $\varphi_{e,max}$. In order to check the demand-capacity ratio for bending moment demands in active links, the nominal moment capacity of the active links can be taken as the $M_{sal}$ = 0.75$M_s$, and bending moment demand ($M^*_{beam}$) is equal the shear demand ($V_e^*$) times half of the active link length. Afterward, the axial force demand in a brace ($N^*_{brace,e}$) is calculated using Equation (B2).

$$N^*_{brace,e} = V_e^* \times \varphi_{e,max} + N^*_{brace,G+\psi cQ} \quad \text{(B2)}$$

where $N^*_{brace,G+\psi cQ}$ is the brace axial force due to gravity loads, the other parameters have been defined previously.

The collector beam has been designed for the Axial ($N^*_{beam}$), bending moment ($M^*_{beam}$), and shear force demands ($V^*_{beam}$). These demands can be computed adopting the following equations.

$$N^*_{beam} = 0.8 \times N^*_{brace} \times \frac{L_{beam}}{L_{brace}} \quad \text{(B3)}$$

$$M^*_{beam} = 0.8 \times V_e^* \varphi_{emax} {}^{e}/_{2} + M^*_{beam(G+\varphi Q)} \quad \text{(B4)}$$

$$V^*_{beam} = V^*_{beam,e} \times \varphi_{e,max} + V_{G+\varphi Q} \quad \text{(B5)}$$

$$V^*_{beam,e} = V_e^* - (V_e^* \times \frac{e/2}{L_{beam}}) \quad \text{(B6)}$$

where $L_{beam}$ and $L_{brace}$ are beam and brace length, respectively; $M^*_{beam(G+\varphi Q)}$ is the beam bending moment due to gravity loads; $e$ is the active link length; $V_{G+\varphi Q}$ is the beam shear demand induced by gravity loads.

Assuming the pined connection at the base of the column and for beam-column joints, the column has been designed only for axial demands ($N^*_{Col,i}$), which is calculated using Equation (B7):

$$N^*_{Col,i} = \sum V_{link,0} + V_{beam,i} + \sum N_{(G+\varphi Q)} \quad \text{(B7)}$$

where $N_{(G+\varphi Q)}$ is the column axial force demands due to gravity loads, the other parameters have been defined previously.

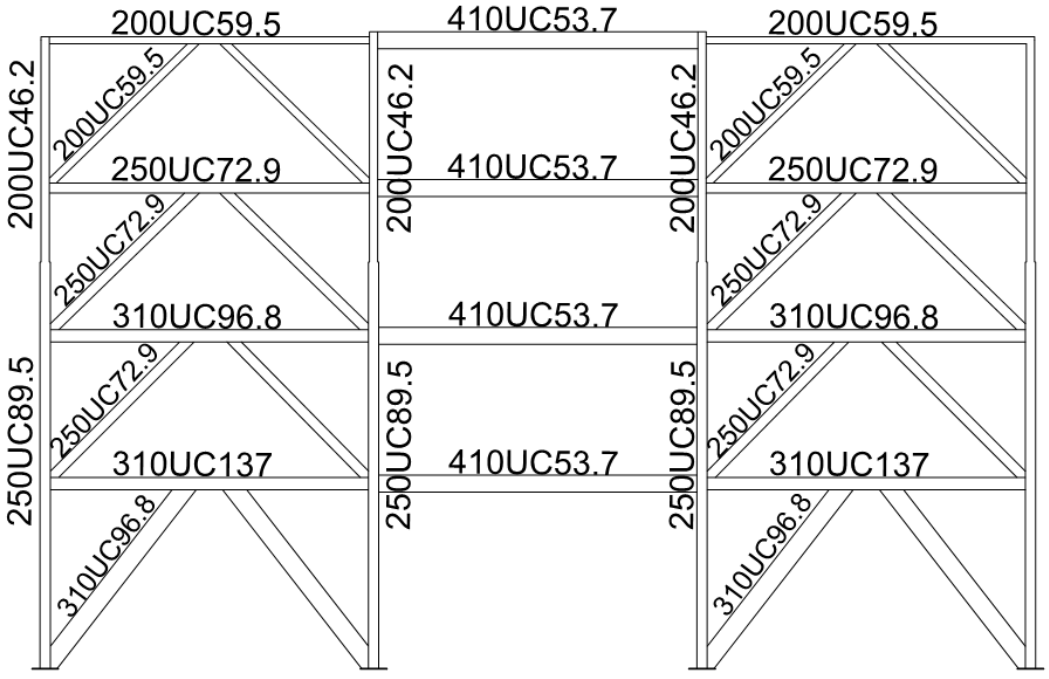


***Figure B.4: Eccentric braced frame's beam and column cross sections.***

## APPENDIX C

This Appendix illustrates the seismic risk calculation carried out for the Christchurch 4-storey case study buildings. Note that the intensity associated with a given limit state exceedance achieved from MSA as explained previously and illustrated in Figure 12. The drift capacity for zero loss and replacement limit state are shown below, as illustrated previously in Figure 16 and Figure 17. The limit states exceedance's intensities were obtained from MSA.

$$\hat{\theta}_{ZL} = 0.17\% \rightarrow \widehat{IM}_{ZL} = 0.14\ g$$
$$\hat{\theta}_{Rep.} = 3\% \rightarrow \widehat{IM}_{Rep} = 1.21\ g$$

Note that the annual rate of exceeding a given intensity can be extracted from the corresponding hazard curve illustrated in part (b) of Figure 21 (displayed below) and Equation (4).

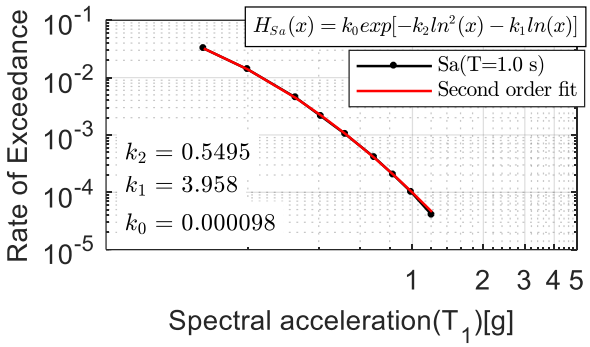


$$\mathrm{H}(S_a) = 0.000098\exp(-0.5495\ln^2(0.14) - 3.958\ln(0.14)) = 0.029$$

$$\mathrm{H}(S_a) = 0.000098\exp(-0.5495\ln^2(1.21) - 3.958\ln(1.21)) = 0.00005$$

The annual rate of exceeding a given limit state can be obtained by applying improved SAC/FEMA approach (Vamvatsikos, 2012) and through Equation (5), Equation (6), and Equation (7). The record to record variability for the zero loss and replacement limit state are found to be 0.3 and 0.47, respectively. For simplicity, however, the uncertainty in capacity was not accounted for.

$$\lambda_{ZL} = \sqrt{0.91}(0.000098)^{1-0.91}[0.029]^{0.91}\exp\left[\frac{3.8231^2}{4 * 0.5495}(1 - 0.91)\right] = 0.032$$

$$p = \frac{1}{1 + 2 * 0.5495 * 0.3^2} = 0.91; \qquad \beta_{Tot} = 0.3$$

Following same procedure as indicated above, the annual rate of exceeding replacement limit state is found to be 0.00017. It can be concluded that equivalent events with 31 and 5882 years return period are expected to cause the zero loss and replacement limit state be exceeded. The expected annual loss can be achieved through Equation (2) assuming that 0.4 is chosen as the replacement threshold loss ratio.

$$EAL = 0.4\frac{\left(\frac{1}{31} - \frac{1.21}{0.14}\frac{1}{5882}\right)}{\left(\frac{1.21}{0.14} - 1\right)\left(1 - \frac{\ln\left(\frac{1.21}{0.14}\right)}{\ln\left(\frac{5882}{31}\right)}\right)} - 0.4\frac{\left(\frac{1}{31} - \frac{1}{5882}\right)}{\left(\frac{1.21}{0.14} - 1\right)} + \frac{1}{5882} =$$

$$EAL = 0.4\frac{(0.0323 - 8.643 * 0.00017)}{(8.6429 - 1)(1 - 0.4111)} - 0.4\frac{(0.0323 - 0.00017)}{(8.643 - 1)} + 0.00017 = 0.12\%$$

In case of choosing the three damage state loss model, one should define the damage control limit state intensity and the associated limit state's rate of exceedance. As demonstrated previously in Table 5, the drift capacity of damage control limit state is found to be 0.7%, the intensity of exceedance of that appears to be 0.4 g, and the corresponding loss ratio is observed to be 3%. The associated limit state rate of exceedance was appeared to be 0.0039 which is equivalent to an event with a return period of 256 years. The aforementioned parameters values are inserted in Equation (3) to compute the expected annual loss, as illustrated below.

$$EAL = 0.03\frac{(0.0323 - 2.857 * 0.0039)}{(2.857 - 1)(1 - \frac{\ln(2.857)}{\ln(8.282)})} - 0.03\frac{(0.0323 - 0.0039)}{(2.857 - 1)} + (0.4 - 0.03)\frac{(3.9e^{-3} - 3.025 * 1.7e^{-4})}{(3.025 - 1)\left(1 - \frac{\ln(3.025)}{\ln(22.94)}\right)} - \left(\frac{0.4 - 0.03}{3.025 - 1} - 0.03\right)(3.9e^{-3} - 1.7e^{-4}) + 1.7e^{-4} = 7e^{-4}$$

If one ignores the uncertainties in demand and capacity, the annual probability of limit state exceedance is obtained equal to the annual probability of exceeding intensity. This leads to a significant underestimation of EAL prediction as indicated in the following.

$$\widehat{IM}_{ZL} = 0.14\ g \rightarrow \mathrm{H}(S_a = 0.14g) = 0.029$$
$$\widehat{IM}_{DC} = 0.40\ g \rightarrow \mathrm{H}(S_a = 0.40g) = 0.023$$
$$\widehat{IM}_{Rep} = 1.21\ g \rightarrow \mathrm{H}(S_a = 1.21g) = 0.00004$$

$$EAL = 0.03\frac{(0.029 - 2.857 * 0.0023)}{(2.857 - 1)(1 - \frac{\ln(2.857)}{\ln(12.09)})} - 0.03\frac{(0.029 - 0.0023)}{(2.857 - 1)} + (0.4 - 0.03)\frac{(2.3e^{-3} - 3.025 * 4.0e^{-5})}{(3.025 - 1)\left(1 - \frac{\ln(3.025)}{\ln(51.41)}\right)} - \left(\frac{0.4 - 0.03}{3.025 - 1} - 0.03\right)(2.3e^{-3} - 4.0e^{-4}) + 1.7e^{-5} = 4.4e^{-4}$$